Eur. Phys. J. A (2014) **50**: 145
DOI 10.1140/epja/i2014-14145-3

THE EUROPEAN PHYSICAL JOURNAL A

Review

Strong coupling effects in near-barrier heavy-ion elastic scattering

N. Keeley[1,a], K.W. Kemper[2,3], and K. Rusek[3]

[1] National Centre for Nuclear Research, ul. Andrzeja Sołtana 7, 05-400 Otwock, Poland
[2] Department of Physics, The Florida State University, Tallahassee, Florida 32306, USA
[3] Heavy Ion Laboratory, University of Warsaw, ul. Pasteura 5a, 02-093 Warsaw, Poland

Received: 20 June 2014 / Revised: 5 August 2014
Published online: 22 September 2014

Communicated by N. Alamanos

Abstract. Accurate elastic scattering angular distribution data measured at bombarding energies just above the Coulomb barrier have shapes that can markedly differ from or be the same as the expected classical Fresnel scattering pattern depending on the structure of the projectile, the target or both. Examples are given such as $^{18}O + ^{184}W$ and $^{16}O + ^{148,152}Sm$, where the expected rise above Rutherford scattering due to Coulomb-nuclear interference is damped by coupling to the target excited states, and the extreme case of ^{11}Li scattering, where coupling to the $^{9}Li + n + n$ continuum leads to an elastic scattering shape that cannot be reproduced by any standard optical model parameter set. An early indication that the projectile structure can modify the elastic scattering angular distribution was the large vector analyzing powers observed in polarised ^{6}Li scattering. The recent availability of high-quality ^{6}He, ^{11}Li and ^{11}Be data provides further examples of the influence that coupling effects can have on elastic scattering. Conditions for strong projectile-target coupling effects are presented with special emphasis on the importance of the beam-target charge combination being large enough to bring about the strong coupling effects. Several measurements are proposed that can lead to further understanding of strong coupling effects by both inelastic excitation and nucleon transfer on near-barrier elastic scattering. A final note on the anomalous nature of ^{8}B elastic scattering is presented as it possesses a more or less normal Fresnel scattering shape whereas one would *a priori* not expect this due to the very low breakup threshold of ^{8}B. The special nature of ^{11}Li is presented as it is predicted that no matter how far above the Coulomb barrier the elastic scattering is measured, its shape will not appear as Fresnel like whereas the elastic scattering of all other loosely bound nuclei studied to date should eventually do so as the incident energy is increased, making both ^{8}B and ^{11}Li truly "exotic".

1 Introduction

Angular distributions of the differential cross section for heavy-ion elastic scattering at incident energies close to the Coulomb barrier, when plotted as a ratio to the Rutherford scattering cross section, typically exhibit the characteristic form often referred to as a Fresnel scattering pattern, *viz.* one or more minor oscillations about the Rutherford value at small angles followed by a larger peak before an essentially exponential fall-off as a function of scattering angle. The large peak is due to interference between scattering from the Coulomb and nuclear potentials and is often referred to as the Coulomb-nuclear interference peak or the Coulomb rainbow peak. As the incident energy is reduced towards the Coulomb barrier the small-angle oscillatory structure and the Coulomb-nuclear interference peak move to larger angles and become less pronounced until they disappear completely: Figure 1 illustrates typical behaviour (optical model calculations are plotted rather than actual data for the sake of clarity).

However, some systems are found to have angular distributions that differ markedly from the norm in that where the Coulomb-nuclear interference peak should be there is instead a large *reduction* of the elastic scattering cross section compared to the Rutherford value. Figure 2 graphically illustrates this phenomenon: Figure 2 (a) shows a normal near-barrier heavy-ion elastic scattering angular distribution, that for 95 MeV ^{16}O incident on a ^{208}Pb target [1], which contrasts with that in fig. 2(b) for 90 MeV ^{18}O incident on a ^{184}W target [2]. The observed depletion of the elastic scattering cross section in the $^{18}O + ^{184}W$ system is due to strong coupling, in this case strong quadrupole Coulomb coupling to the first 2^+ excited state of ^{184}W [2]. Similar effects have also been observed due to strong quadrupole Coulomb coupling in the projectile in the $^{20}Ne + ^{208}Pb$ system [3]. It is these strong

[a] e-mail: nicholas.keeley@fuw.edu.pl

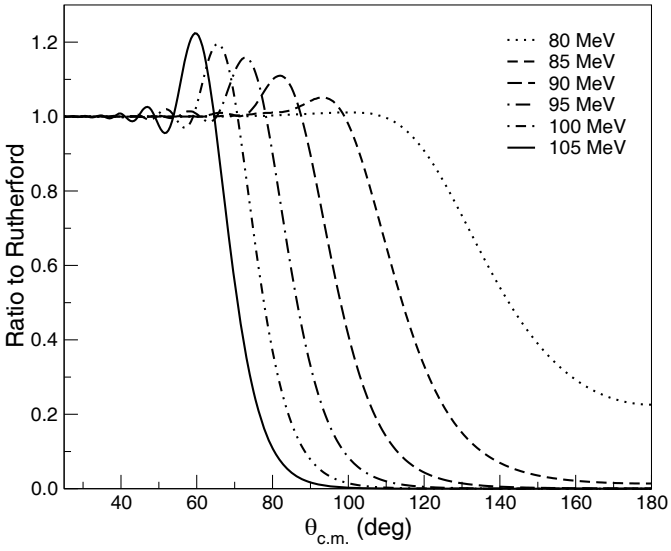

Fig. 1. Elastic scattering angular distributions for the $^{16}O + ^{208}Pb$ system at several near-barrier incident energies calculated using the optical model. Optical potential parameters were taken from a fit to the data of ref. [1]. The nominal Coulomb barrier for this system corresponds to an incident energy of about 83 MeV.

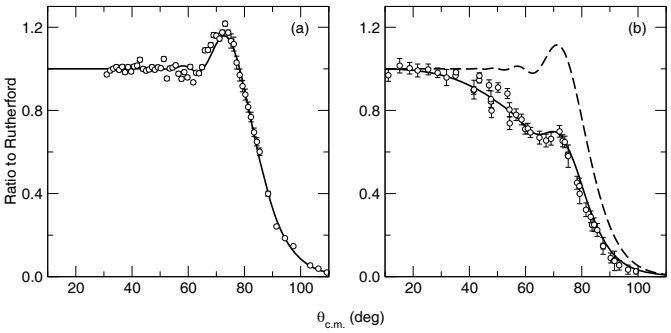

Fig. 2. (a) Elastic scattering angular distribution for 95 MeV ^{16}O incident on a ^{208}Pb target. The circles represent the data of ref. [1] (renormalised to the Rutherford value at forward angles on this plot) while the solid curve represents an optical model fit. (b) Elastic scattering angular distribution for 90 MeV ^{18}O incident on a ^{184}W target. The circles represent the data of ref. [2] while the solid curve denotes the result of a coupled channels calculation including Coulomb and nuclear coupling to the first 2^+ excited state of ^{184}W. The dashed curve denotes the result of a no coupling optical model calculation using the same optical potential as in the coupled channels calculation.

coupling effects on the elastic scattering angular distribution that form the subject of this review. Such a review is timely, since with the increasing quality of radioactive beams, rather precise measurements of angular distributions of the elastic scattering of exotic nuclei are now feasible and it is possible to probe the projectile structure through such scattering. Such measurements have already been made for several weakly bound exotic nuclei and the resulting angular distributions are found to exhibit all the characteristics of strong coupling effects, in these cases due to strong coupling to the projectile continuum.

Note that in both figures we have plotted the cross section on a linear scale rather than the more usual logarithmic one. In this we follow the recommendation of Satchler [4,5] who pointed out that a semi-logarithmic plot can obscure the details of the nuclear-Coulomb interference region, the part of the angular distribution most sensitive to the nuclear interaction: "A particularly sensitive part of the angular distribution is the oscillatory region just before the exponential fall below the Rutherford cross section. (The details of this region may be overlooked if, as is often done, the ratio-to-Rutherford cross section is shown on a semi-logarithmic plot. It is more revealing to use a linear plot.)" [5].

We begin with a survey of elastic scattering measurements for systems involving stable nuclei that exhibit strong coupling effects from both inelastic and transfer couplings. This survey aims to be representative rather than exhaustive, in that we give examples of the types of system that exhibit strong coupling effects. We then review measurements of the elastic scattering of exotic nuclei that also exhibit strong coupling effects before summarising the necessary conditions for the existence of these effects. Finally we make some suggestions for future measurements along with the accuracy required to explore further this phenomenon.

2 Strong coupling effects with stable beams

2.1 Systems with effects due to target coupling

The first published data to show strong coupling effects on the elastic scattering were for the ^{18}O and $^{12}C + ^{184}W$ systems at incident energies of 90 and 70 MeV, respectively, [2]. As can be seen in fig. 3 the effect is less marked for the $^{12}C + ^{184}W$ data, due to the smaller charge product for this projectile, although the ^{12}C incident energy is somewhat higher with respect to the Coulomb barrier than for the $^{18}O + ^{184}W$ data and this will also play a rôle in reducing the effect. Also shown in fig. 3 is the measured angular distribution for the elastic scattering of a 90 MeV ^{18}O beam from a ^{208}Pb target which exhibits the usual Fresnel shape, providing further proof that the strong coupling effect is due to the ^{184}W target and not the projectile. Incidentally, a comparison of fig. 2 and fig. 3 well illustrates the value of presenting near-barrier heavy-ion elastic scattering angular distributions on a linear scale.

These data were taken with the use of a QDDD magnetic spectrometer in order to obtain the resolution necessary to separate inelastic scattering to the 111 keV 2^+_1 first excited state of ^{184}W from the elastic scattering. As Thorn *et al.* [2] were careful to point out, previous measurements of the "elastic scattering" of heavy ions from heavy deformed targets obtained the usual Fresnel scattering angular distributions because they could not resolve inelastic scattering to the ground state rotational bands. Thorn *et al.* also showed, by explicit coupled channels calculations, that the elastic scattering data can be well

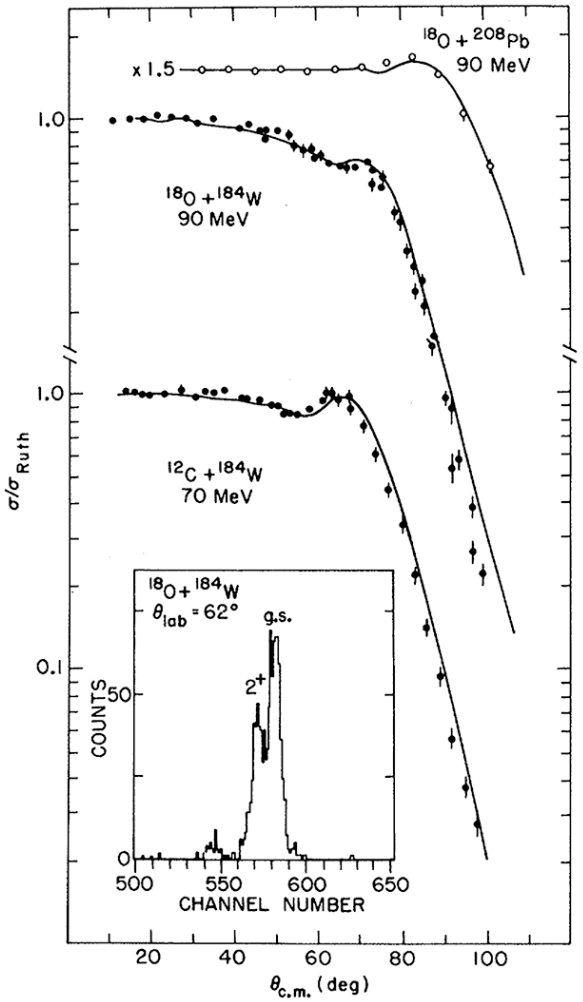

Fig. 3. Elastic scattering data for the $^{18}O + ^{184}W$ and $^{12}C + ^{184}W$ systems at 90 and 70 MeV, respectively. The solid curves denote the results of optical model ($^{18}O + ^{208}Pb$) or coupled channels ($^{18}O + ^{184}W$ and $^{12}C + ^{184}W$) calculations. Taken from ref. [2]. Reprinted fig. 1 with permission from [2]. © 1977, The American Physical Society.

described by coupling to the 111 keV 2_1^+ state of ^{184}W, the effect on the elastic scattering being almost entirely due to the Coulomb coupling (it should be noted that these elastic scattering data cannot be described by conventional optical model potentials).

Angular distributions for the elastic scattering of 72 MeV ^{16}O ions from ^{152}Sm [6,7] and, to a lesser extent from ^{148}Sm [7] show similar behaviour, see fig. 4. Again, the main source of the effects on the elastic scattering angular distribution is Coulomb excitation of the first 2^+ excited states of the targets, although as Kim points out [6], nuclear couplings are important for a detailed reproduction of both the elastic and inelastic scattering angular distributions. Data were also obtained at lower energies for the $^{16}O + ^{148,150,152}Sm$ systems by Talon *et al.* [8]. These data too show significant deviations from Rutherford scattering but the effect on the shape of the angular distribution is not so dramatic as for the higher-

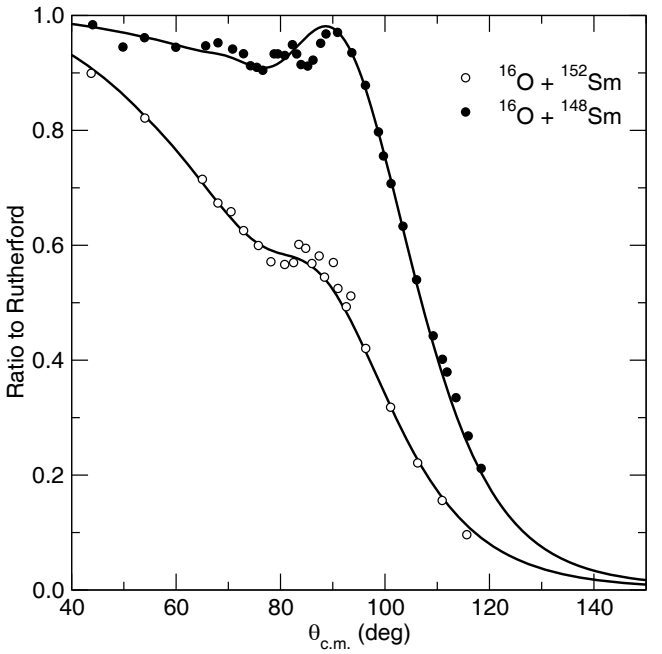

Fig. 4. Elastic scattering data for the $^{16}O + ^{148,152}Sm$ systems at incident energies of 72 MeV. The data are taken from ref. [7]. The solid curves denote the result of coupled channels calculations including $0^+ \longleftrightarrow 2^+ \longleftrightarrow 4^+$ rotational model coupling.

energy data. Details of the experimental procedure for the 72 MeV $^{16}O + ^{148,152}Sm$ measurements are not given in refs. [6,7] but the lower-energy measurements of Talon *et al.* [8] employed a QDDD magnetic spectrometer.

Figure 4 provides an unambiguous demonstration of the link between the importance of the coupling effect and the strength of the $B(E2)$ and the excitation energy of the 2_1^+ state since the charge products and, to a very good approximation, the Coulomb barriers are identical for the $^{16}O + ^{148}Sm$ and ^{152}Sm systems. While both these Sm isotopes are deformed, ^{152}Sm has a $B(E2; 0_1^+ \rightarrow 2_1^+)$ nearly five times that of ^{148}Sm plus a much lower excitation energy. This is confirmed by the 72.3 MeV $^{16}O + ^{144}Sm$ elastic scattering data of Abriola *et al.* [9] which show a classic Fresnel scattering angular distribution, ^{144}Sm being a weakly coupled spherical nucleus with a relatively high-lying first excited state.

The above examples demonstrate that, under the right conditions, strong coupling to low-lying excited states of the target can give rise to near-barrier elastic scattering angular distributions that deviate significantly from the usual Fresnel pattern. We shall explore fully what these conditions are in a later section. For the present, suffice it to say that all systems where the effect has been observed and has been ascribed to target couplings involve heavy deformed target nuclei.

2.2 Systems with effects due to projectile coupling

Elastic scattering angular distributions for the $^{20}Ne + ^{208}Pb$ system have been measured for incident ^{20}Ne

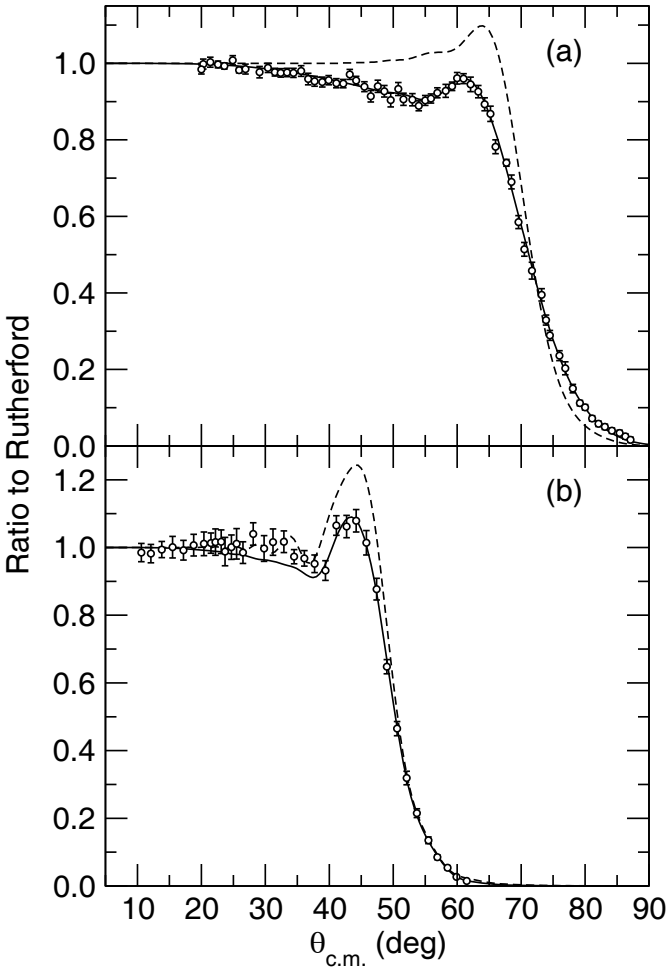

Fig. 5. Elastic scattering data for the $^{20}\mathrm{Ne} + {}^{208}\mathrm{Pb}$ system at incident energies of 131 MeV (a) and 161.2 MeV (b). Data are taken from refs. [3] and [5] respectively. The solid curves denote the results of coupled channels calculations including coupling to the 2_1^+ state of ^{20}Ne. The dashed curves denote the results of no coupling optical model calculations using the same optical potentials as in the appropriate coupled channels calculations.

energies of 161.2 MeV [5] and 131 MeV [3]. The 161.2 MeV data at first sight appear to show the usual Fresnel scattering pattern and an acceptable description of these data could be obtained with standard optical potentials, with the exception of the angular region between 34° and 50° [5]. The 131 MeV data, however, unambiguously show the strong coupling effect, the shape of the angular distribution being similar to that for the $^{16}\mathrm{O} + {}^{148}\mathrm{Sm}$ system (cf. figs. 4 and 5). Both data sets were obtained using position-sensitive silicon detectors mounted on moveable arms. Coupled channels calculations reveal that the dip in the elastic scattering angular distribution just before the main Coulomb-nuclear interference peak at 161.2 MeV is a residual effect due to the strong coupling to the ^{20}Ne 2_1^+ state, see fig. 5(b). These data therefore clearly show that the strong coupling effect diminishes as the incident energy is increased.

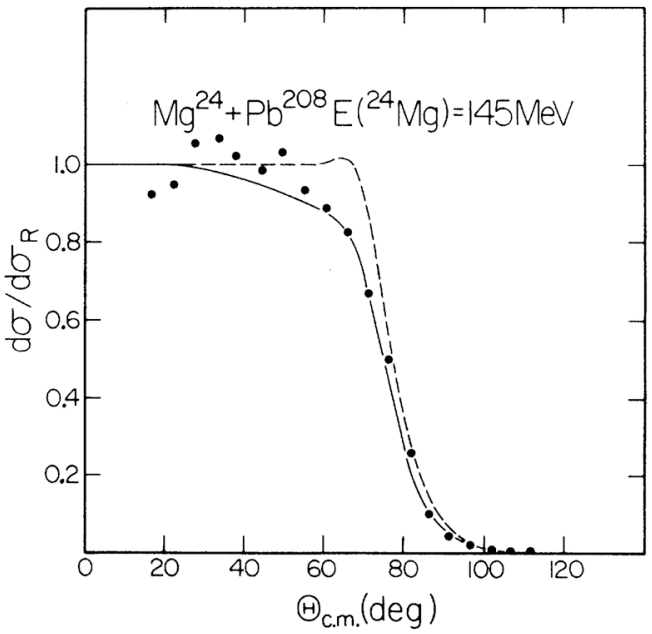

Fig. 6. Elastic scattering data for the $^{24}\mathrm{Mg} + {}^{208}\mathrm{Pb}$ system at an incident energy of 145 MeV. The solid curve denotes an optical model fit including a long-range polarisation potential due to Coulomb excitation of the 2_1^+ of ^{24}Mg while the dashed curve indicates the result of an optical model calculation with the same potential but without the Coulomb polarisation potential. Taken from ref. [10]. Reprinted fig. 4 with permission from [10]. © 1981, The American Physical Society.

Elastic scattering angular distributions have also been measured for the $^{24}\mathrm{Mg} + {}^{208}\mathrm{Pb}$ and $^{26}\mathrm{Mg} + {}^{208}\mathrm{Pb}$ systems at incident energies of 145 MeV [10] and 200 MeV [11] and 200 MeV [12], respectively. The 145 MeV $^{24}\mathrm{Mg} + {}^{208}\mathrm{Pb}$ data were taken using an Enge split pole magnetic spectrometer but both sets of 200 MeV data employed standard position sensitive silicon detectors. The 200 MeV data have elastic scattering angular distributions of similar shape to that for the 161.2 MeV $^{20}\mathrm{Ne} + {}^{208}\mathrm{Pb}$ data, *i.e.* there is only a residual strong coupling effect, this time clearly visible as a distinct dip in the cross section just before the main Coulomb-nuclear interference peak. The effect is smaller for ^{26}Mg, as might be expected due to its weaker collectivity compared to ^{24}Mg. The 145 MeV $^{24}\mathrm{Mg} + {}^{208}\mathrm{Pb}$ data clearly show the strong coupling effect, see fig. 6.

Our final example of a system with strong coupling effects due to the projectile is $^{28}\mathrm{Si} + {}^{208}\mathrm{Pb}$. Elastic scattering data for this system are available at incident energies of 162 MeV [10], 166 MeV [13], 209.8 MeV [14] and 225 MeV [15]. The influence of strong coupling is apparent for all these data sets although the effect becomes weaker as the incident energy is increased. The measurements of refs. [10,13,15] were made using Enge split pole spectrometers while that of ref. [14] employed a QDDD spectrometer.

For all these systems it is strong Coulomb coupling to the 2_1^+ excited state of the projectile that is predominantly

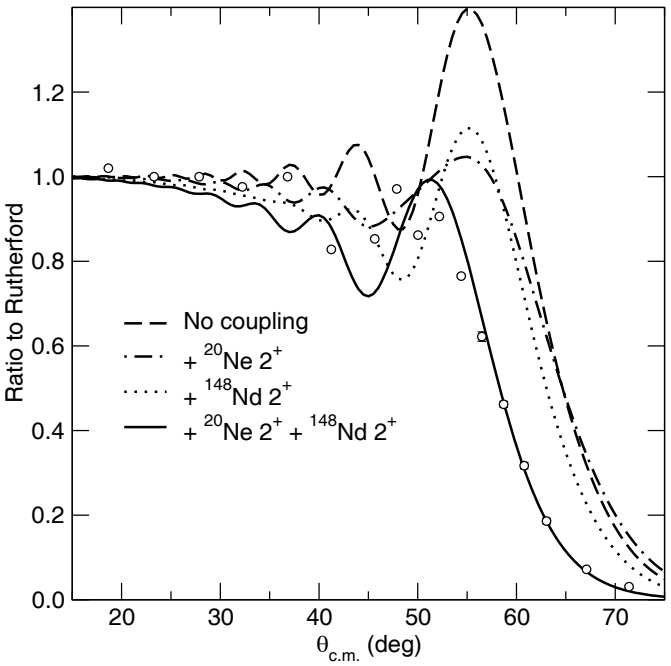

Fig. 7. Elastic scattering data for the $^{20}\mathrm{Ne} + {}^{148}\mathrm{Nd}$ system at an incident energy of 116 MeV. The data are taken from ref. [16]. The solid curve denotes the result of a coupled channels calculation including both ^{20}Ne and ^{148}Nd $0_1^+ \rightarrow 2_1^+$ coupling (but no mutual excitation), the dotted curve the result of a calculation including the ^{148}Nd $0_1^+ \rightarrow 2_1^+$ coupling only, the dot-dashed curve a calculation including the ^{20}Ne $0_1^+ \rightarrow 2_1^+$ coupling only and the dashed curve the no coupling calculation.

responsible for the strong coupling effect on the elastic scattering, similarly to what was found for the systems with strongly coupled targets. This raises the intriguing question as to what the angular distribution for a system with a strongly deformed projectile *and* a strongly deformed target would look like.

2.3 Systems with effects due to projectile and target coupling

As an example of a system with strong coupling in both projectile and target we cite $^{20}\mathrm{Ne} + {}^{148}\mathrm{Nd}$. Data for the elastic and inelastic scattering in this system were measured using a QDDD magnetic spectrometer at an incident energy of 116 MeV [16]. The shape of the angular distribution is similar to those for systems with strong coupling in either the target alone or the projectile alone, thus the presence of strong coupling in both target and projectile does not seem to affect the qualitative nature of its effect on the elastic scattering, see fig. 7.

In spite of a large cross section for mutual excitation of the ^{20}Ne and ^{148}Nd 2_1^+ states it was found that coupling to mutual excitation had little influence on the elastic scattering angular distribution [16]. The effect seems to be due to the individual couplings to the separate 2_1^+ states, although the calculations plotted in fig. 7 suggest that the combined effect of projectile and target couplings is greater than the sum of its parts.

2.4 Strong coupling effects with polarised projectiles

An example of a different type of strong coupling effect is provided by the analysing powers for elastic scattering of polarised heavy ion beams. Analysing powers measured in experiments with polarised beams were found to be even more sensitive to the coupling effects than the cross sections. In the 1980s many experiments with polarised ^{6,7}Li and ^{23}Na beams were performed at the Max Planck Institute for Nuclear Physics in Heidelberg, Germany [17]. Later on these studies were moved to the Nuclear Structure Facility of the Daresbury Laboratory, U.K., and in the second part of the 1990s to the Florida State University, U.S.A. The very first experiments with vector polarised ^{6}Li beams scattered from nickel targets already revealed large values of the vector analysing powers (iT_{11}) that could not be explained by a "static" spin-orbit interaction derived from the deuteron-target or the nucleon-nucleon spin-orbit potentials by means of folding methods. The analysing powers predicted by optical model calculations with spin-orbit interactions calculated in this way were much too small to explain the experimental data.

The explanation of this "spin crisis" came from microscopic coupled channels calculations that included couplings to the 3^+ resonant first excited state of ^{6}Li [18]. In fig. 8 the $^6\mathrm{Li} + {}^{58}\mathrm{Ni}$ elastic scattering data (angular distributions of the differential cross section and the vector analysing powers) taken from [19] are compared with the model predictions. The short-dashed curves represent the results of an optical model calculation with the spin-orbit potential derived from the deuteron-target interaction by means of the Watanabe-type cluster-folding method. This calculation underpredicted the measured differential cross section and generated values of the analysing power that are very close to zero. Inclusion of couplings to the resonant first excited state of the projectile in coupled channels calculations produced much larger values of the analysing powers, close to experiment (solid curves). The inclusion of further couplings to the resonances at 4.31 and 5.65 MeV excitation energy improved the description of the data still further (dashed curves). Further improvement would require couplings to the non-resonant $\alpha + d$ continuum.

This is illustrated in fig. 9. The experimental data for 60 MeV polarised $^6\mathrm{Li} + {}^{26}\mathrm{Mg}$ elastic scattering were obtained at the Nuclear Structure Facility of the Daresbury Laboratory [20]. As in the previous case, optical model calculations with the cluster-folded spin-orbit potential included generated negligible values of the vector analysing power (dotted curves). Couplings to all three resonances of ^{6}Li improved the description of the differential cross section angular distribution and produced sizable values of the analysing power (dashed curves). Finally, inclusion of couplings to the non-resonant continuum resulted in a good reproduction of both sets of data (solid curves). One should mention that these calculations were free of any adjustable parameters.

Finally, in ref. [21] an extensive coupled channels analysis of $^6\mathrm{Li} + {}^{12}\mathrm{C}$ and $^6\mathrm{Li} + {}^{16}\mathrm{O}$ elastic and inelastic scattering data found that for these light target systems the

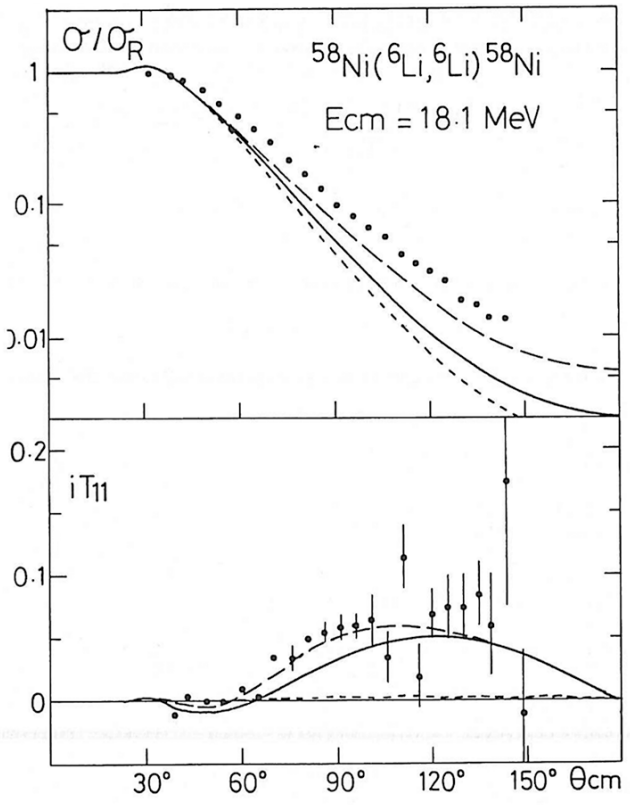

Fig. 8. Elastic scattering angular distributions for polarised $^{6}\mathrm{Li} + {}^{58}\mathrm{Ni}$ compared to optical model and coupled channels calculations. The analysing powers are almost completely generated by the coupling to the 3^+ resonant state of ^{6}Li. Taken from ref. [18], fig. 5.

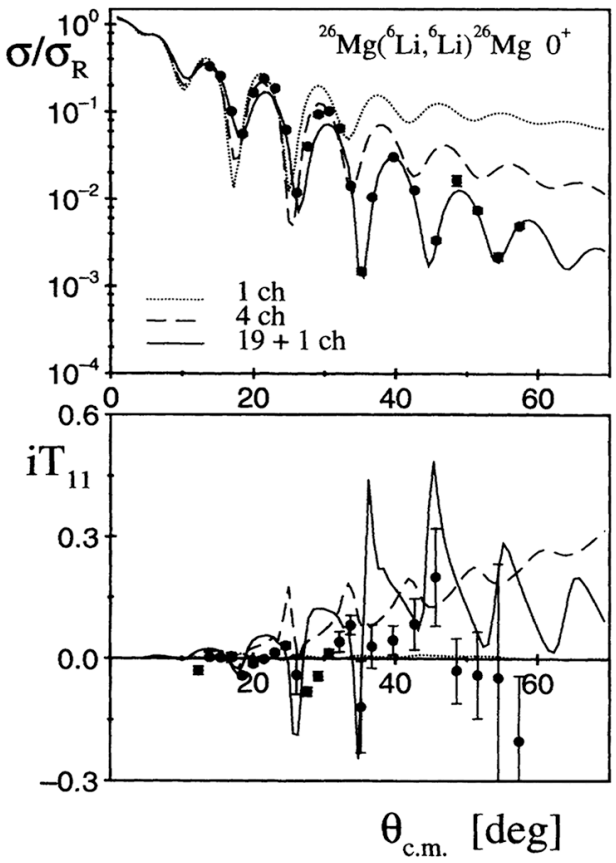

Fig. 9. Comparison of 60 MeV $^{6}\mathrm{Li} + {}^{26}\mathrm{Mg}$ elastic scattering data with the results of coupled channels calculations. The dotted curves denote the result of an optical model calculation including a cluster-folded spin-orbit potential, the dashed curves denote the result of a coupled channels calculation including couplings to all three ^{6}Li resonant states and the solid curves denote the result of a coupled discretised continuum channels calculation including couplings to the non-resonant $\alpha + d$ continuum. Note that the analysing power arises entirely from channel couplings. Taken from ref. [20]. Reprinted fig. 3 with permission from [20]. © 1994, The American Physical Society.

elastic scattering vector analysing power could only be satisfactorily explained by explicitly including couplings to the $L = 2$ resonances of ^{6}Li. However, it was found that the static spin-orbit potential did have an influence on the final result for the calculated analysing power for these systems via a complicated interference with the dynamic coupling effects.

2.5 Strong coupling effects without strong couplings

The title of this final sub-section dealing with strong coupling effects on elastic scattering involving stable heavy-ion beams would appear at first sight to be something of a paradox: how is it possible to have a "strong coupling" effect on the elastic scattering in the absence of strong couplings? However, this phenomenon does occur. Neither ^{58}Ni nor ^{64}Ni are considered to exhibit strong coupling, their relatively high-lying 2_1^+ levels ($E_\mathrm{x} = 1.45$ MeV for ^{58}Ni and 1.35 MeV for ^{64}Ni) being rather weakly coupled vibrational states. The elastic scattering data of ref. [22] for the $^{58}\mathrm{Ni} + {}^{64}\mathrm{Ni}$ system at two near-barrier energies nevertheless show the characteristic "strong coupling" form rather than the usual Fresnel scattering pattern, see fig. 10. The apparent paradox may be resolved by considering the large charge product for this system which transforms the weak coupling of the Ni 2_1^+ levels into a strong Coulomb coupling.

Similar effects should be exhibited by the near-barrier elastic scattering of most weakly coupled medium mass vibrational nuclei from a sufficiently heavy target. This indeed seems to be the case, see *e.g.* the $^{40}\mathrm{Ar} + {}^{208}\mathrm{Pb}$ elastic scattering data of ref. [23] and the $^{58}\mathrm{Ni} + {}^{208}\mathrm{Pb}$ data of ref. [24]. However, a possible exception is the $^{40}\mathrm{Ca} + {}^{208}\mathrm{Pb}$ system. A quasi-elastic scattering angular distribution for this system has been reported for an incident ^{40}Ca energy of 236 MeV [25]. While it is not explicitly stated in ref. [25] exactly which channels are included in the definition of "quasi-elastic" the angular distribution does exhibit the shape associated with strong coupling effects, from which we may infer that the elastic scattering angular

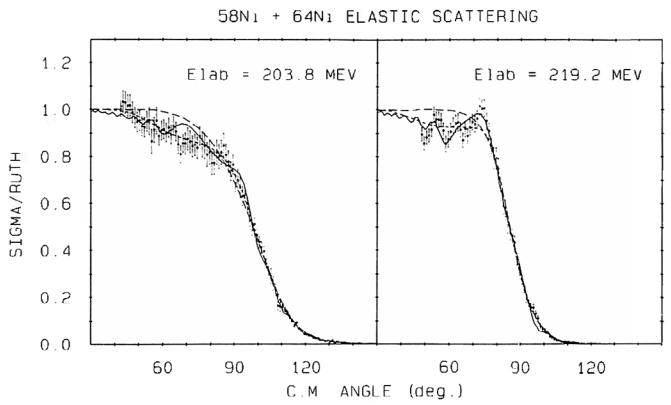

Fig. 10. Elastic scattering data for the $^{58}\mathrm{Ni} + ^{64}\mathrm{Ni}$ system at incident energies of 203.8 MeV (left) and 219.2 MeV (right). The solid curves denote coupled channels calculations including coupling to the 2_1^+ states of both nuclei while the dashed curves are optical model calculations. Taken from ref. [22], fig. 4.

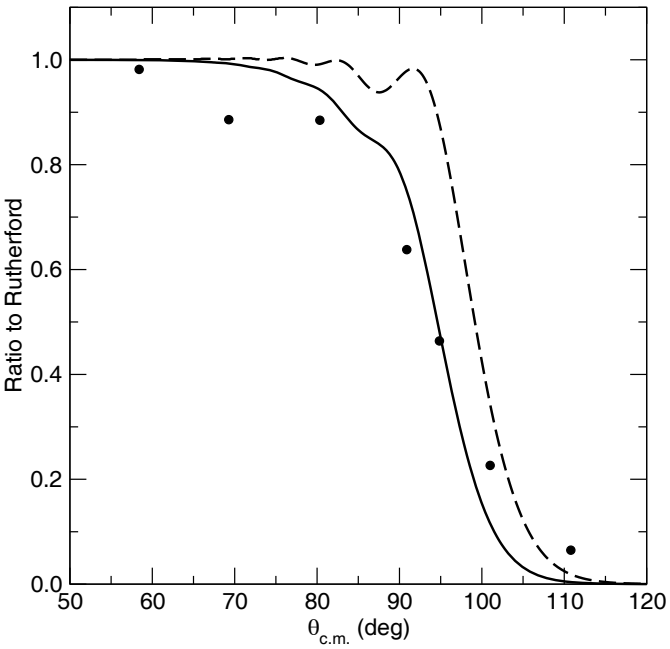

Fig. 11. Calculated elastic scattering angular distributions for the $^{40}\mathrm{Ca} + ^{208}\mathrm{Pb}$ system at an incident energy of 236 MeV for the no coupling (dashed curve) and coupled reaction channels (solid curve) cases. The coupled reaction channels calculation includes couplings to the $^{208}\mathrm{Pb}(^{40}\mathrm{Ca}, ^{41}\mathrm{Ca})^{207}\mathrm{Pb}$ single neutron pickup reaction only. The points denote the quasi-elastic scattering data of ref. [25].

distribution will also do so. However, coupled channels calculations suggest that, due to the doubly magic nature of ^{40}Ca and its consequent structure properties, the effect is not produced by inelastic couplings. Rather, it appears that this system may be a case where strong transfer couplings produce a similar effect on the elastic scattering. Calculations presented in ref. [25] seem to bear this out and conventional coupled reaction channels calculations including the $^{208}\mathrm{Pb}(^{40}\mathrm{Ca}, ^{41}\mathrm{Ca})^{207}\mathrm{Pb}$ single neutron pickup coupling confirm this, see fig. 11.

3 Strong coupling effects with radioactive beams

The elastic scattering of certain light, weakly bound radioactive nuclei from heavy targets has also been found to exhibit the non-Fresnel pattern angular distributions characteristic of strong coupling effects. For these nuclei it is strong coupling to the low-lying continuum that is responsible. A general review of available data for light radioactive beams was given in ref. [26] so that we shall only give representative examples here.

A particularly good example of the effect of strong coupling to the low-lying continuum on the near-barrier elastic scattering of a weakly bound radioactive nucleus is the $^6\mathrm{He} + ^{208}\mathrm{Pb}$ system. Figure 12(a) shows the 27 MeV $^6\mathrm{He} + ^{208}\mathrm{Pb}$ elastic scattering angular distribution of Kakuee *et al.* [27]. Coupled discretised continuum channels calculations have confirmed that the effect is dominated by Coulomb dipole coupling to the low-lying $\alpha + n + n$ continuum. However, since this is a strong Coulomb coupling effect the charge product of the projectile-target system must be sufficiently large for the effect to be observed; the $^6\mathrm{He} + ^{64}\mathrm{Zn}$ data of refs. [28,29] exhibit the classic Fresnel shape. This question was examined further in ref. [30] where a series of coupled discretised continuum channels calculations suggested that a target with an atomic number greater than about 80 was required in order unambiguously to see the strong coupling effect. Figure 12(b) underlines that careful selection of the incident energy is also required if the strong coupling effect is to be observed; if the energy is too high with respect to the nominal Coulomb barrier then even for a ^{208}Pb target the ^{6}He elastic scattering is expected to present a more or less conventional Fresnel type shape (45 MeV represents an incident energy approximately 2.5 times that equivalent to the nominal Coulomb barrier for the $^6\mathrm{He} + ^{208}\mathrm{Pb}$ system).

Preliminary data for the elastic scattering of ^{8}He from a ^{208}Pb target at an incident energy of 22 MeV have recently been published [31]. They show a similar shape to the $^6\mathrm{He} + ^{208}\mathrm{Pb}$ data at the same incident energy [32], although given the higher breakup thresholds of ^{8}He, combined with a considerably larger spectroscopic factor for single-neutron removal, coupling to neutron stripping reactions may turn out to have a more prominent rôle in ^{8}He elastic scattering than in ^{6}He where its effect is most important at large angles, see, *e.g.*, ref. [33].

The elastic scattering of ^{11}Li from ^{208}Pb at near- and sub-barrier energies has recently been measured and shows spectacular departures from the Fresnel shape [34]. This too has been shown to be due mostly to strong Coulomb dipole coupling to the low-lying continuum. The coupling effect is much stronger than for ^{6}He, in part due to the extra charge on the ^{11}Li nucleus but mostly due to the much stronger Coulomb dipole polarisability of ^{11}Li [35]. Figure 13 plots the data for 29.8 MeV $^{11}\mathrm{Li} + ^{208}\mathrm{Pb}$ elastic

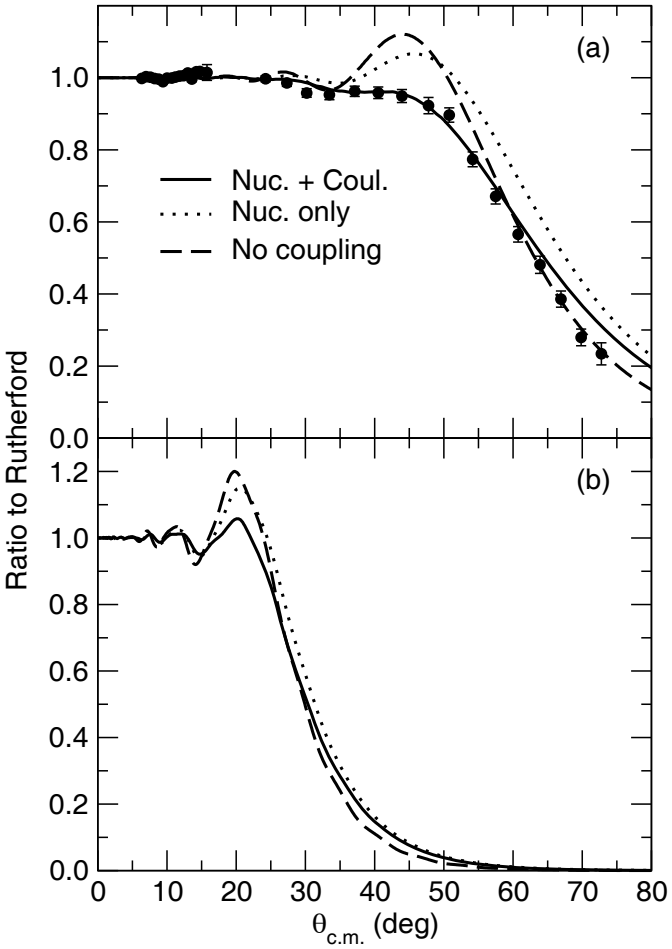

Fig. 12. (a) Elastic scattering angular distribution for the $^{6}\mathrm{He} + {}^{208}\mathrm{Pb}$ system at an incident energy of 27 MeV. The solid curve denotes a coupled discretised continuum channels calculation while the dashed curve denotes the corresponding no coupling optical model calculation. The dotted curve denotes the result of a coupled discretised continuum channels calculation with nuclear coupling only (but including diagonal Coulomb potentials). The data are taken from ref. [27]. (b) The solid curve denotes a coupled discretised continuum channels calculation of the $^{6}\mathrm{He} + {}^{208}\mathrm{Pb}$ elastic scattering at an incident ^{6}He energy of 45 MeV while the dashed curve denotes the corresponding no coupling optical model calculation. The dotted curve denotes the result of a coupled discretised continuum channels calculation with nuclear coupling only (but including diagonal Coulomb potentials).

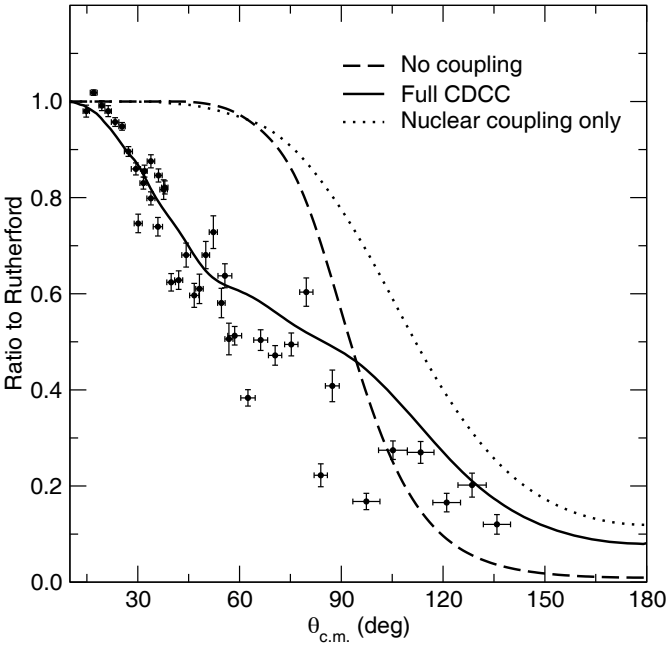

Fig. 13. Elastic scattering angular distribution for the $^{11}\mathrm{Li} + {}^{208}\mathrm{Pb}$ system at an incident energy of 29.8 MeV. The solid and dashed curves denote the results of coupled discretised continuum channels and no coupling calculations, respectively. The dotted curve shows the result of a coupled discretised continuum channels calculation with nuclear coupling only (but including diagonal Coulomb potentials). The data are taken from ref. [34]. Adapted from ref. [35], fig. 1.

scattering compared to a coupled discretised continuum channels calculation. The great importance of Coulomb couplings may be seen by comparing the solid and dotted curves in the figure, nuclear coupling only becoming important for angles greater than about 80°.

Quasi-elastic scattering data for the $^{11}\mathrm{Be} + {}^{64}\mathrm{Zn}$ system have been measured at an incident energy of 28.7 MeV [36]. The data are quasi-elastic since inelastic scattering to the low-lying bound first excited state of ^{11}Be could not be separated from the elastic scattering, although for most practical purposes they may be regarded as pure elastic. For this system, and unlike the case for the $^{6}\mathrm{He} + {}^{64}\mathrm{Zn}$ elastic scattering [28,29], the angular distribution has the characteristic shape associated with strong coupling effects. The persistence of strong coupling effects for elastic scattering from a medium mass target could partly be due to the extra charge on the ^{11}Be nucleus compared to ^{6}He. However, coupled discretised continuum channels calculations found that, unlike all the other systems mentioned in this review, strong *nuclear* couplings —in this case to the low-lying $^{10}\mathrm{Be} + n$ continuum— appeared to have the most important influence on the ^{11}Be elastic scattering [37], see fig. 14. The exact importance of the nuclear couplings is to some extent model dependent, see ref. [38]. However, it is clear that the nuclear couplings are far more important than for ^{6}He or ^{11}Li (or, indeed for the strongly coupled systems involving stable nuclei) and are vital in reproducing the shape of the angular distribution. The calculations of refs. [37] and [38] both neglect the possibility of excitation of the ^{10}Be core. Extensions of the standard coupled discretised continuum channels technique have been developed to include core excitation effects [39–41] and have recently been applied to these data [41]. It was found that the standard coupled discretised continuum channels calculations of ref. [38] gave similar results for the quasi-elastic scattering to those of the more sophisticated model including core excitation [41] although the latter was in better agreement with the inclusive breakup cross section data.

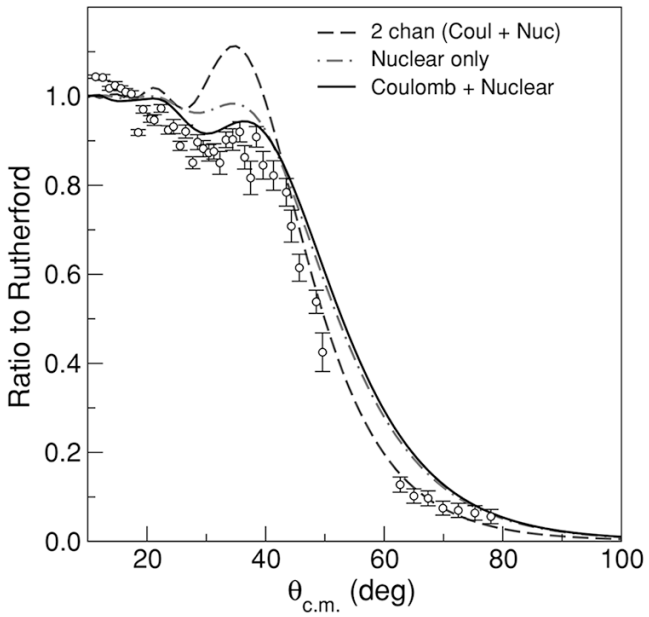

Fig. 14. Quasi-elastic scattering angular distribution for the ^{11}Be + ^{64}Zn system at an incident energy of 28.7 MeV. The solid curve denotes the result of the full coupled discretised continuum channels calculation including both Coulomb and nuclear couplings, while the dot-dashed curve denotes the result of a similar calculation but with nuclear couplings only while retaining the diagonal Coulomb potentials. The dashed curve is the result of a calculation including coupling (both Coulomb and nuclear) to the 320 keV $1/2^-$ first excited state of ^{11}Be only. Taken from ref. [37]. Reprinted fig. 3 with permission from [37]. © 2010, The American Physical Society.

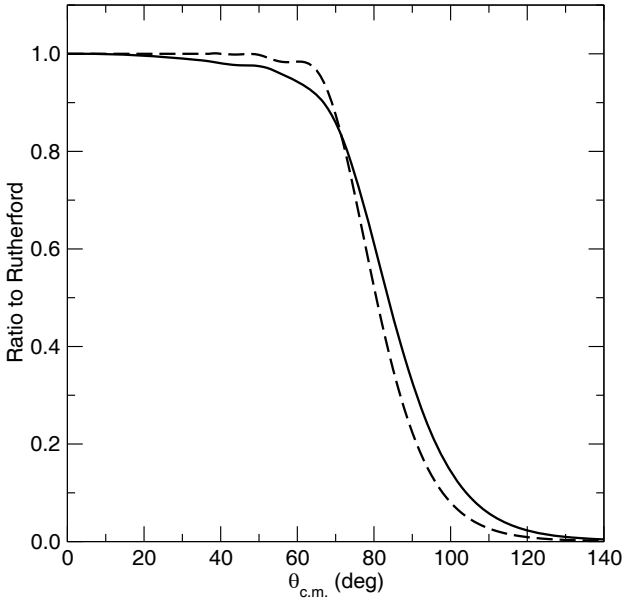

Fig. 15. Elastic scattering angular distribution for the ^{8}B + ^{208}Pb system at an incident energy of 60 MeV. The full curve denotes the result of a coupled discretised continuum channels calculation while the dashed curve represents the result of the no coupling optical model calculation. Adapted from fig. 25 of ref. [26] (see ref. [26] for details of the calculation).

We end this brief survey of strong coupling effects for systems involving radioactive beams with another paradox. In this case it is a nucleus that would be expected *a priori* to show such effects in its elastic scattering but which apparently does not, ^{8}B. The threshold against $^{8}\mathrm{B} \rightarrow {}^{7}\mathrm{Be} + p$ breakup is just 137.5 keV so that the cross section for this process should be large and one would naively expect commensurate effects on the elastic scattering due to coupling to the continuum. However, coupled discretised continuum channels calculations suggest that the influence on the elastic scattering of coupling to the $^{7}\mathrm{Be} + p$ continuum is small, even for a ^{208}Pb target [26], see fig. 15. While the model of ^{8}B employed in these calculations is simplified to the extent that excitations of the ^{7}Be core are ignored, the 170.3 MeV $^{8}\mathrm{B} + {}^{\mathrm{Nat}}\mathrm{Pb}$ elastic scattering data of Yang *et al.* [42] suggest that it is sufficiently realistic. Coupling effects are expected to be minimal at this energy —approximately three times the Coulomb barrier— and indeed the measured angular distribution shows a classic Fresnel scattering pattern [42]. However, calculations for near-barrier energies suggest that any suppression of the nuclear-Coulomb interference peak for $^{8}\mathrm{B} + {}^{208}\mathrm{Pb}$ elastic scattering will be due largely to "static" effects rather than coupling to the continuum [26]. This is borne out by similar calculations [43] for the near-barrier $^{8}\mathrm{B} + {}^{58}\mathrm{Ni}$ data of ref. [44]. Unfortunately ^{8}B is a difficult beam to produce, particularly at lower energies, so that the available near-barrier data do not have a sufficient number of points to confirm this experimentally [44].

Part of the explanation for this behaviour may come from the fact that in ^{8}B the "valence" particle is a proton rather than a neutron, thus allowing subtle interference effects involving the Coulomb interaction with the core in addition to the presence of a Coulomb barrier tending to suppress the large radius tail of the valence particle wave function. Indeed, Kumar and Bonaccorso [45] have shown that with regard to the nuclear breakup the proton in ^{8}B behaves like a more tightly bound neutron. Later work showed the importance of interference effects for breakup observables [46]. Nevertheless, the charge on the proton does not seem to account entirely for the lack of coupling effect on the near-barrier ^{8}B elastic scattering, since coupling to breakup has a much larger effect for ^{6}Li elastic scattering at similar energies with respect to the Coulomb barrier in spite of the very much larger breakup threshold (and consequently much smaller breakup cross section) for this projectile compared to ^{8}B, see, for example, ref. [47].

4 Conditions governing strong coupling effects

4.1 General considerations

In this section we explore the conditions necessary for strong coupling effects on near-barrier elastic scattering to manifest themselves. In the previous two sections we

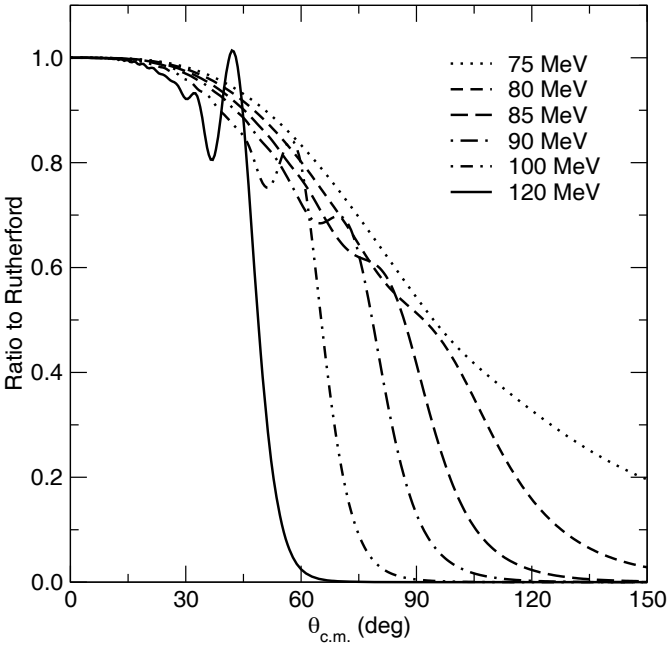

Fig. 16. Coupled channels calculations for the $^{18}O + ^{184}W$ system at several sub- and near-barrier bombarding energies. The input parameters are identical with those of the coupled channels calculations in ref. [2]. The nominal Coulomb barrier for this system corresponds to a bombarding energy of about 77.7 MeV.

have seen how systems with strong coupling exhibit near-barrier elastic scattering angular distributions of a characteristic shape that, at first sight, appears to have nothing in common with the usual Fresnel-type elastic scattering pattern. However, like the conventional Fresnel pattern the strong coupling angular distribution shape does evolve as a function of bombarding energy, see, for example, the $^{28}Si + ^{208}Pb$ data of refs. [10,13–15]. In order to illustrate this more clearly we present in fig. 16 a series of coupled channels calculations for the $^{18}O + ^{184}W$ system at incident energies ranging from somewhat below the nominal Coulomb barrier ($V_B = 70.8$ MeV, equivalent to a bombarding energy of about 77.7 MeV) to approximately $1.5 \times V_B$. The calculations use the same optical potential and coupling parameters as those of ref. [2] since in this figure we are investigating the qualitative evolution of the shape of the angular distribution as a function of bombarding energy rather than attempting to make quantitatively accurate predictions of the elastic scattering at a particular energy.

A comparison with fig. 1 will show that, despite the superficially completely different shapes of the elastic scattering angular distributions for the strongly coupled system, what we find in fig. 16 is in fact a standard Fresnel-type scattering pattern superimposed on a strong Coulomb coupling angular distribution shape. As the bombarding energy is increased from 75 MeV we see an evolution from a completely structureless angular distribution to the emergence of a strong Coulomb-nuclear interference peak as the real nuclear potential becomes of more importance, exactly as in the classic Fresnel scattering pattern. The difference in the strongly coupled system is that now, due to depletion of the elastic scattering by the strong Coulomb excitation, the Coulomb-nuclear interference maximum is peaked at much less than the Rutherford value, except for energies considerably above the Coulomb barrier.

4.2 Strong coupling equivalent to a long-range DPP

Thus far we have explained strong coupling effects in terms of coupled channels calculations. However, on publication of the $^{18}O + ^{184}W$ data of Thorn *et al.* [2] it was almost immediately demonstrated that they could also be explained in terms of a long-range dynamic polarisation potential (DPP) induced by the Coulomb coupling which, when added to a conventional optical model potential, provided a good description of the data. This DPP could easily be calculated from a single parameter, the $B(E\lambda)$ value, making use of some approximations [48–51]. The formalism of Baltz *et al.* [50,51] is more sophisticated than that of Love *et al.* [48,49] although both give similar results. There is now a considerable literature on the calculation using various approximations of Coulomb excitation DPPs and their application to elastic scattering data, most recently including radioactive beam data.

Love *et al.* and Baltz *et al.* assume the sudden approximation, which leads to a predominantly imaginary DPP (the real parts of their DPPs are in fact negligible) and most subsequent work on Coulomb DPPs has made similar assumptions. However, if the adiabatic approximation is appropriate, *i.e.* if the collision time $\gg$ the period of internal motion, a purely real, attractive DPP results [52]. In reality, the DPP will be complex and the real and imaginary parts of the DPPs extracted from coupled discretised continuum channels calculations for light weakly bound nuclei are usually comparable in size, see, *e.g.*, ref. [53]. The form of the real part of such DPPs at large radii matches very well the adiabatic model expression for the (purely real) DPP which is directly related to the polarisability of the weakly bound nucleus. The dipole polarisability of light weakly bound nuclei may thus be obtained from fits to the real part of the DPP extracted from appropriate coupled discretised continuum channels calculations, see for example refs. [35] and [54]. Starting from analytic expressions for the imaginary polarisation potential for Coulomb dipole excitation, the corresponding real polarisation potential has been obtained through a dispersion relation involving the Coulomb dipole excitation energy [55], thus yielding an analytic expression for a complex Coulomb dipole DPP. This formalism was applied to the $^{11}Li + ^{208}Pb$ elastic scattering at 50 MeV, producing a prediction for the angular distribution in remarkable qualitative agreement with the recent measurements at somewhat lower incident ^{11}Li energies [34].

While coupled channels calculations are now routine, at least for stable nuclei where the number of states involved is small, the expressions for the Coulomb DPPs do give valuable insight into the conditions necessary for

strong coupling effects to be maximal. For example, Love *et al.* [49], referring to their expression for the Coulomb DPP state that it: "... provides an explicit guide as to when coupling to a particular inelastic channel may be important. Clearly, the effects should be most important in those cases in which the target and/or projectile has a large $B(E\lambda)$ and the projectile and/or the target possesses a large Z."

4.3 The conditions under which strong coupling effects are expected

This leads us conveniently into a discussion of the necessary conditions under which strong coupling effects on the near-barrier elastic scattering are expected to appear. Frahn and Hill [56] have given an excellent summary of how the strong coupling influence depends on various parameters which we may conveniently quote here: "... based solely on the long-ranged nature of the polarization potential ... some general predictions could be made:

i) Dynamic polarization causes an overall reduction of the differential cross section which is small at small angles and becomes gradually stronger with increasing θ.
ii) The polarization probability increases rapidly with increasing deformation of the target and/or projectile.
iii) For a given ratio of the energy to the Coulomb barrier energy, the polarization increases strongly with the mass numbers of projectile and target.
iv) For a given projectile-target system the polarization effect diminishes rapidly with increasing energy."

to which we might also add the excitation energy of the strongly coupled state; even a strongly coupled state will not produce the characteristic strong coupling elastic scattering angular distribution if its excitation energy is high. This is, of course, a somewhat subjective statement since whether or not the strong coupling effect is present also depends on the incident energy. However, since such effects are usually limited to incident energies relatively close to the Coulomb barrier states with excitation energies of approximately 5–10 MeV would not be expected to have much influence on the elastic scattering in the relevant energy regime regardless of their coupling strength. A proper investigation of the interplay of these two linked properties —excitation energy of the coupled state(s) and projectile incident energy— is beyond the scope of the present review but would form an interesting subject for further study.

Summarising the above information, we would expect strong coupling effects to be present in the near-barrier elastic scattering under the following circumstances:

1) Systems where the target is a well-deformed medium-to-heavy mass nucleus with a low-lying (a few hundred keV or less) first excited state. In this instance the projectile may be a relatively light, more or less inert nucleus such as ^{12}C or ^{16}O or similar, the only requirement being that the charge product is sufficiently large since the Coulomb coupling effect is dominant in such systems. If the target is sufficiently heavy, *i.e.* it carries a large enough charge, even α particle elastic scattering should show the strong coupling effect under these circumstances, see, for example refs. [49,57].
2) Systems where the projectile is a well-deformed light nucleus with a strongly coupled ground state rotational band and the target is a heavy inert nucleus (^{208}Pb or similar). Again, since the coupling effect is Coulomb dominated exactly how heavy the target nucleus needs to be for the effect to be plain will depend on the projectile charge. In this case the first excited state of the deformed projectile need not be particularly low-lying (1–2 MeV is sufficient).
3) Systems where the projectile is a well-deformed light nucleus and the target a well-deformed medium-to-heavy mass nucleus. It appears that coupling to mutual excitation of the target and projectile has little or no influence on the elastic scattering in these systems although the overall effect of individual coupling to the projectile and target excited states does seem to be greater than the sum of its parts.
4) Systems where both the projectile and target are of medium mass or greater. In this case the nuclei involved may have only relatively weak couplings but the system will still exhibit strong coupling effects on the elastic scattering due to the large charge product. Any medium mass (or greater) nucleus incident on, say, a ^{208}Pb target should give rise to the characteristic strong coupling shape for its near barrier elastic scattering. Doubly magic medium mass nuclei may prove exceptions, cf. ^{40}Ca.
5) Systems with weakly bound radioactive beams incident on heavy targets such as ^{197}Au and ^{208}Pb. There are two caveats to this statement: a weak binding energy does not automatically guarantee the existence of the strong coupling effect, as the case of ^{8}B proves and a heavy target may not always be necessary to see the effect, cf. ^{11}Be and ^{11}Li.
6) Well angular momentum and Q value matched transfer reactions can give similar strong coupling effects to those due to strong inelastic couplings. Such couplings may turn out to be important for exotic nuclei.

In all these cases it should also be emphasised that the optimum effect will be for energies somewhat greater than the Coulomb barrier, about 20–30% greater than $V_{\rm B}$.

Finally, to illustrate further the importance of excitation energy on the strong coupling effect at a given incident energy close to the Coulomb barrier we present in fig. 17 test coupled channels calculations for the $\alpha + {}^{238}$U system at a bombarding energy of 24.7 MeV. The calculations are similar to those of Rusek [57] except that for our purposes we have only included coupling to the 2_1^+ state of ^{238}U (omission of coupling to the other members of the ground state band has little effect on the result beyond damping out the small scale oscillations about the Rutherford value at small angles). The actual excitation energy of the 2_1^+ state, 45 keV, was multiplied by factors of 10, 50 and 100 in order to investigate the influence of

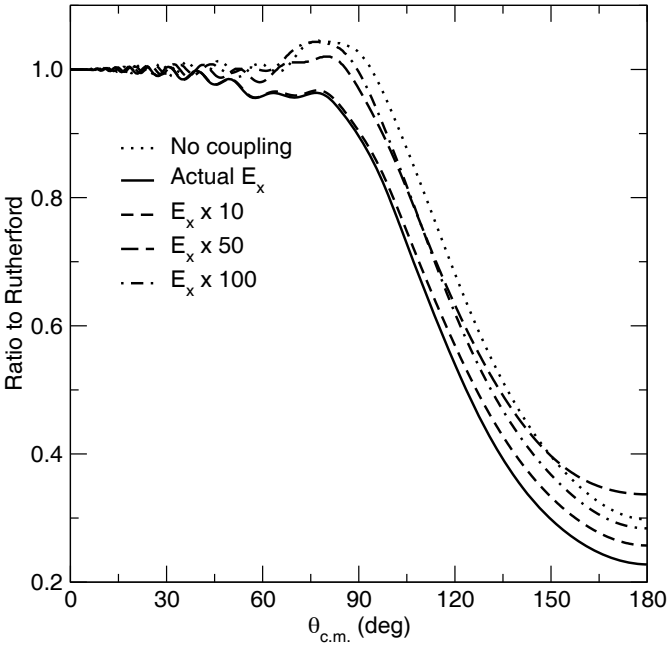

Fig. 17. Coupled channels calculations for the $\alpha + {}^{238}$U system at a bombarding energy of 24.7 MeV. The various curves correspond to a no coupling optical model calculation (dotted curve) and coupled channels calculations with the excitation energy of the ^{238}U 2_1^+ state multiplied by factors of 1, 10, 50 and 100.

excitation energy on the strong coupling effect. It is found that the excitation energy has to be multiplied by a factor of about 30, *i.e.* an excitation energy of 1.35 MeV, before the characteristic strong coupling shape has more or less disappeared in favour of the usual Fresnel-type elastic scattering pattern. Although there are still significant coupling effects for $E_{\rm x} \times 50$ and 100 they are of such a nature that they could be subsumed into the optical model fitting procedure. These calculations demonstrate that even a strongly coupled state will not give rise to the characteristic strong coupling elastic scattering angular distribution shape if its excitation energy is too high, although exactly what constitutes "too high" may also depend on other factors such as the projectile incident energy.

5 Suggested future experiments

In this section we propose systems that would be interesting candidates for further study of the strong coupling effect in the light of our conclusions concerning the conditions under which such effects should be most important. Suggestions are made for experiments with both stable and radioactive beams and an indication of the required precision of the measurements is given. We have limited ourselves to what we hope are practical measurements, either already or in the near future. All coupled channels calculations in the following subsections were performed using the code FRESCO [58].

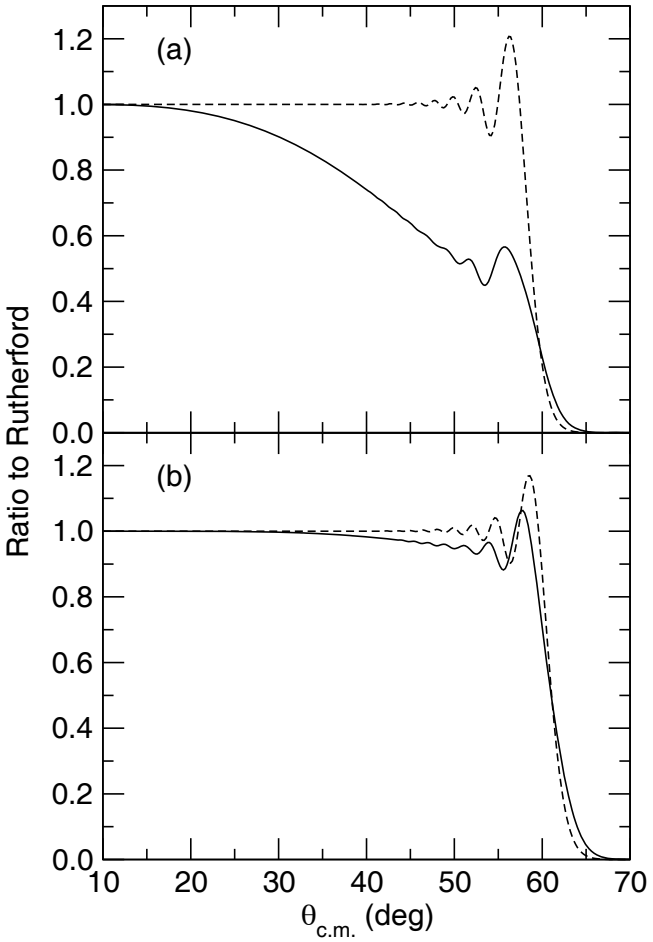

Fig. 18. (a) Coupled channels calculation for the $^{120}\mathrm{Sn} + {}^{208}\mathrm{Pb}$ system at a bombarding energy of 900 MeV. The calculation including Coulomb and nuclear couplings to the 2_1^+ state of ^{120}Sn and the 3_1^- state of ^{208}Pb is denoted by the solid curve while the dashed curve denotes the result of the no coupling optical model calculation. (b) Coupled channels calculation for the $^{132}\mathrm{Sn} + {}^{208}\mathrm{Pb}$ system at a bombarding energy of 900 MeV. The calculation including Coulomb and nuclear couplings to the 2_1^+ state of ^{132}Sn and the 3_1^- state of ^{208}Pb is denoted by the solid curve while the dashed curve denotes the result of the no coupling optical model calculation.

5.1 Heavy beams on a heavy target

Due to what we might term the magnifying effect of the large charge product, the elastic scattering of a heavy nucleus from a similarly heavy target ought, in principle, to provide a good example of the "strong coupling effect without strong coupling." As an example, we suggest the $^{120}\mathrm{Sn} + {}^{208}\mathrm{Pb}$ system. Measurement of the pure elastic scattering would require a detection energy resolution of about 1 MeV in order to resolve inelastic scattering to the first excited state of ^{120}Sn ($E_{\rm x} = 1.17$ MeV). An incident ^{120}Sn energy of 900 MeV should be suitable, thus a detection energy resolution of about 0.1% would be required.

We present the result of a coupled channels calculation for a 900 MeV ^{120}Sn beam incident on a ^{208}Pb target in fig. 18(a). The calculation does not aim at

a quantitatively accurate prediction of the angular distribution but it should be reasonably realistic. The optical potential was calculated according to the prescription of Broglia and Winther [59] with the imaginary part taken to be the same as the real part but with a depth divided by a factor of 4. The $B(E2)$ and $B(E3)$ values were taken from Raman *et al.* [60] and Kibédi and Spear [61], respectively. The nuclear deformation lengths were derived from the $B(E\lambda)$ values assuming the collective model and radii of $1.2 \times A^{1/3}$ fm. A precision of $\pm 5\%$ on each point of the angular distribution would be more than sufficient not only to demonstrate the effect but also show the details of the structure, provided that a sufficient number of points could be measured. Such a measurement should therefore be feasible over a reasonable period of time given the availability of a suitable ^{120}Sn beam.

By way of contrast, in fig. 18(b) we present the result of a coupled channels calculation for the radioactive ^{132}Sn beam incident on a ^{208}Pb target, again at an incident energy of 900 MeV. The ^{132}Sn nucleus is doubly magic and its first excited state, a 2^+ level, is consequently situated at the rather high energy of 4.04 MeV. We would therefore anticipate a much reduced strong coupling effect. The calculation suggests that this will indeed be the case, at least as far as inelastic excitations are concerned; in fact, the residual "strong coupling" effect is almost entirely due to coupling to the ^{208}Pb 3_1^- state. The coupled channels calculation took the $B(E2)$ value for ^{132}Sn from Pritychenko *et al.* [62], the nuclear deformation length being derived in a similar fashion to those in the $^{120}\mathrm{Sn} + {}^{208}\mathrm{Pb}$ calculation. The optical potential was again calculated using the prescription of Broglia and Winther [59]. In this case a detection energy resolution of about 0.25% would be required, since it would be necessary to resolve the 3_1^- state of ^{208}Pb ($E_\mathrm{x} = 2.61$ MeV) in order to measure pure elastic scattering. A precision of $\pm 5\%$ on each point of the angular distribution would be more than adequate to demonstrate the predicted difference between the $^{120}\mathrm{Sn} + {}^{208}\mathrm{Pb}$ and $^{132}\mathrm{Sn} + {}^{208}\mathrm{Pb}$ elastic scattering. Such a measurement should therefore be a feasible radioactive beam experiment.

5.2 Deformed beams on a heavy deformed target

We have already seen in subsect. 2.3 that systems involving a deformed light nucleus incident on a deformed heavy target lead to interesting results with effects due to strong coupling in both the projectile and the target. It would be of interest to extend these studies to a more strongly coupled target such as ^{184}W for instance in order to check whether what we might term the "greater than the sum of its parts effect" is universal. Suitable beams for this purpose would be ^{20}Ne and ^{24}Mg or ^{28}Si. Sufficient energy resolution to measure pure elastic scattering would require the use of a spectrometer to detect the scattered beam particles but this ought to be possible since a detection energy resolution of about 100 keV would be necessary to separate the first excited state of ^{184}W.

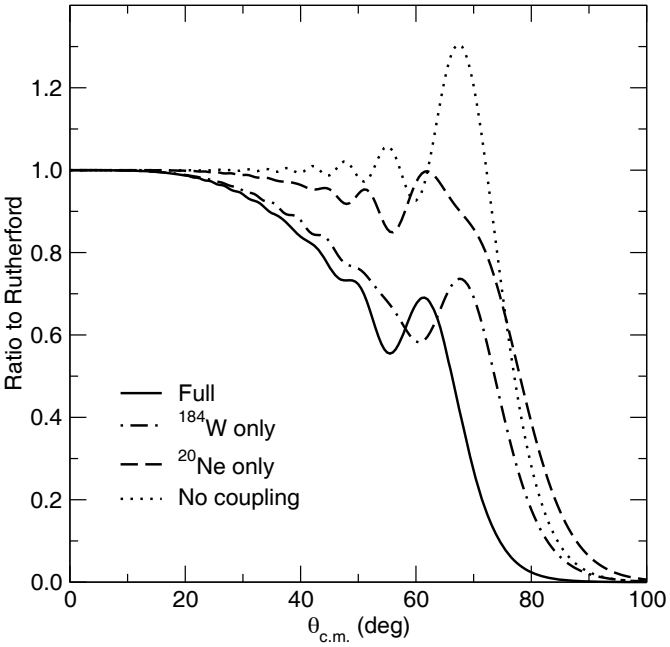

Fig. 19. Coupled channels calculations for the $^{20}\mathrm{Ne} + {}^{184}\mathrm{W}$ system at a bombarding energy of 120 MeV. The dotted curve denotes the no coupling optical model calculation, the dashed curve a coupled channels calculation including coupling to the ^{20}Ne 2_1^+ state only, the dot-dashed curve a coupled channels calculation including coupling to the ^{184}W 2_1^+ state only and the solid curve the full coupled channels calculation including coupling to both target and projectile 2_1^+ states (but not mutual excitation).

In fig. 19 we plot the results of coupled channels calculations for the $^{20}\mathrm{Ne} + {}^{184}\mathrm{W}$ system at a bombarding energy of 120 MeV, about 23% higher than the nominal Coulomb barrier for this system. The calculations again employed the Broglia-Winther prescription for the optical model parameters, the imaginary potential depth being set at a quarter of the real depth. The $B(E2)$ values were taken from ref. [60] and the nuclear deformation lengths were taken from refs. [3] and [2] for ^{20}Ne and ^{184}W, respectively. In this system, unlike the $^{20}\mathrm{Ne} + {}^{148}\mathrm{Nd}$ data of [16], the coupling effect is dominated by the target coupling (to be expected since the coupling effect is much stronger in ^{184}W). However, the calculations also suggest that the overall coupling effect is not "greater than the sum of its parts" in this case, thus making it an interesting system for further experimental investigation.

As a second example we take the $^{24}\mathrm{Mg} + {}^{184}\mathrm{W}$ system at an incident ^{24}Mg energy of 145 MeV, again about 23% greater than the nominal Coulomb barrier for this system. Coupled channels calculations similar to those just described for the $^{20}\mathrm{Ne} + {}^{184}\mathrm{W}$ system are presented in fig. 20. The $B(E2)$ value for ^{24}Mg was taken from ref. [60] and the corresponding nuclear deformation length was taken from ref. [10]. The coupling effect is again dominated by the target coupling and seems to show similar behaviour to $^{20}\mathrm{Ne} + {}^{184}\mathrm{W}$ with regard to the cumulative effect of coupling to target and projectile states.

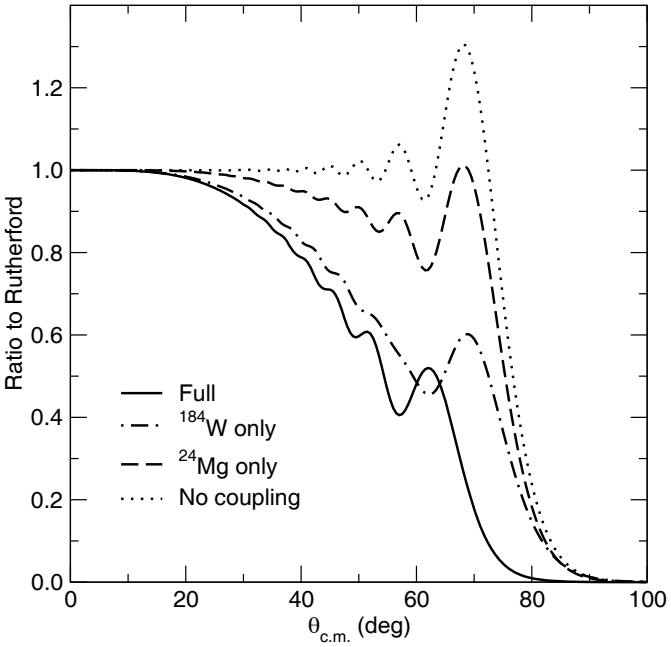

Fig. 20. Coupled channels calculations for the $^{24}\mathrm{Mg} + {}^{184}\mathrm{W}$ system at a bombarding energy of 145 MeV. The dotted curve denotes the no coupling optical model calculation, the dashed curve a coupled channels calculation including coupling to the $^{24}\mathrm{Mg}$ 2_1^+ state only, the dot-dashed curve a coupled channels calculation including coupling to the $^{184}\mathrm{W}$ 2_1^+ state only and the solid curve the full coupled channels calculation including coupling to both target and projectile 2_1^+ states (but not mutual excitation).

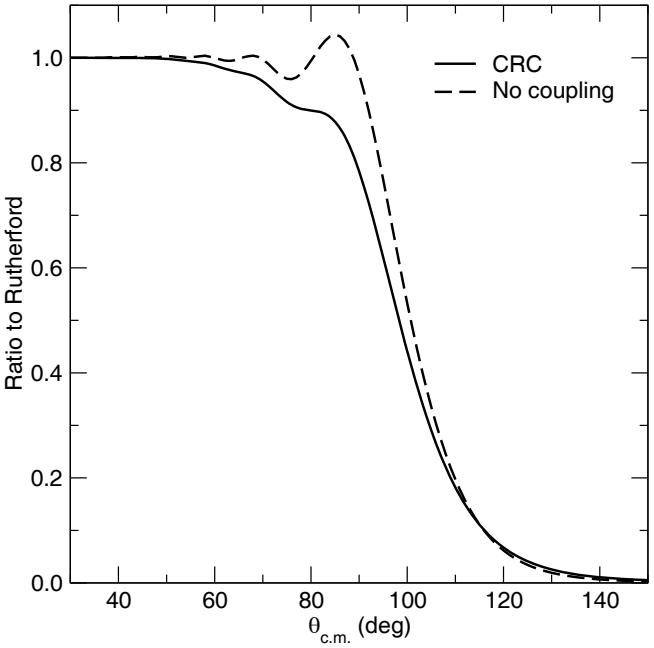

Fig. 21. Coupled reaction channels calculation for the $^{15}\mathrm{C} + {}^{208}\mathrm{Pb}$ system at a bombarding energy of 65 MeV. The dashed curve denotes the no coupling optical model calculation while the solid curve denotes the coupled reaction channels calculation including coupling to the $^{208}\mathrm{Pb}(^{15}\mathrm{C}, {}^{14}\mathrm{C})^{209}\mathrm{Pb}$ single neutron stripping.

It is interesting to note that in both these cases where the target coupling effect is predicted to dominate there appears to be a destructive interference effect between projectile and target coupling influences. This would certainly bear further investigation and good elastic scattering data (at the ± 5% level) for these systems are desirable. Both experiments should be feasible with currently available beams provided access to a spectrometer is possible in order to obtain the required detection energy resolution of about 100 keV.

5.3 Light weakly bound radioactive beam on a heavy target

While experiments to measure the near-barrier elastic scattering of light weakly bound radioactive beams from heavy targets have already been performed for many projectiles of interest, as outlined in sect. 3, there remain a few systems which should prove interesting and which have not yet been studied. One such system should be $^{15}\mathrm{C} + {}^{208}\mathrm{Pb}$. The $^{15}\mathrm{C}$ nucleus is relatively weakly bound, its threshold against $^{15}\mathrm{C} \rightarrow {}^{14}\mathrm{C} + n$ breakup being 1.218 MeV. However, perhaps the most important aspect of its structure is that it is a single neutron halo nucleus with the valence neutron in a $2s_{1/2}$ orbital, thus raising the intriguing possibility of strong coupling effects due to neutron stripping because of the long tail on the wave function of the valence neutron. Coupled reaction channels calculations have already demonstrated that the $^{208}\mathrm{Pb}(^{15}\mathrm{C}, {}^{14}\mathrm{C})^{209}\mathrm{Pb}$ single neutron stripping reaction should have a significant coupling effect on sub-barrier $^{15}\mathrm{C} + {}^{208}\mathrm{Pb}$ elastic scattering [63].

In fig. 21 we present a coupled reaction channels calculation showing the effect of coupling to the single neutron stripping reaction on the $^{15}\mathrm{C} + {}^{208}\mathrm{Pb}$ elastic scattering angular distribution for an incident $^{15}\mathrm{C}$ energy of 65 MeV. The entrance channel $^{15}\mathrm{C} + {}^{208}\mathrm{Pb}$ optical potential was obtained by Watanabe-type cluster folding of $^{14}\mathrm{C} + {}^{208}\mathrm{Pb}$ and $n + {}^{208}\mathrm{Pb}$ optical potentials over the internal wave function of the $^{15}\mathrm{C}$ ground state. The $^{15}\mathrm{C}$ wave function was calculated assuming a Woods-Saxon well of "standard" geometry: $R_0 = 1.25 \times \mathrm{A}^{1/3}$ fm, $a = 0.65$ fm, the well depth being adjusted to give the correct single neutron binding energy, and a spin-orbit component of the same geometry with a fixed well depth of 6 MeV. No attempt was made to tune these parameters. The $^{14}\mathrm{C} + {}^{208}\mathrm{Pb}$ potential parameters were taken from a fit to the $^{12}\mathrm{C} + {}^{208}\mathrm{Pb}$ data of ref. [64] nearest to the appropriate energy using the potential geometry of ref. [5] and adjusting the real and imaginary depths. The neutron potential was the central part of pot I of ref. [65]. The exit channel $^{14}\mathrm{C} + {}^{209}\mathrm{Pb}$ potential parameters were taken from a similar fit to the appropriate data of ref. [64] to those used to generate the entrance channel potential. The $\langle {}^{15}\mathrm{C} | {}^{14}\mathrm{C} + n \rangle$ and $\langle {}^{209}\mathrm{Pb} | {}^{208}\mathrm{Pb} + n \rangle$ overlaps and spectroscopic factors were as in ref. [63].

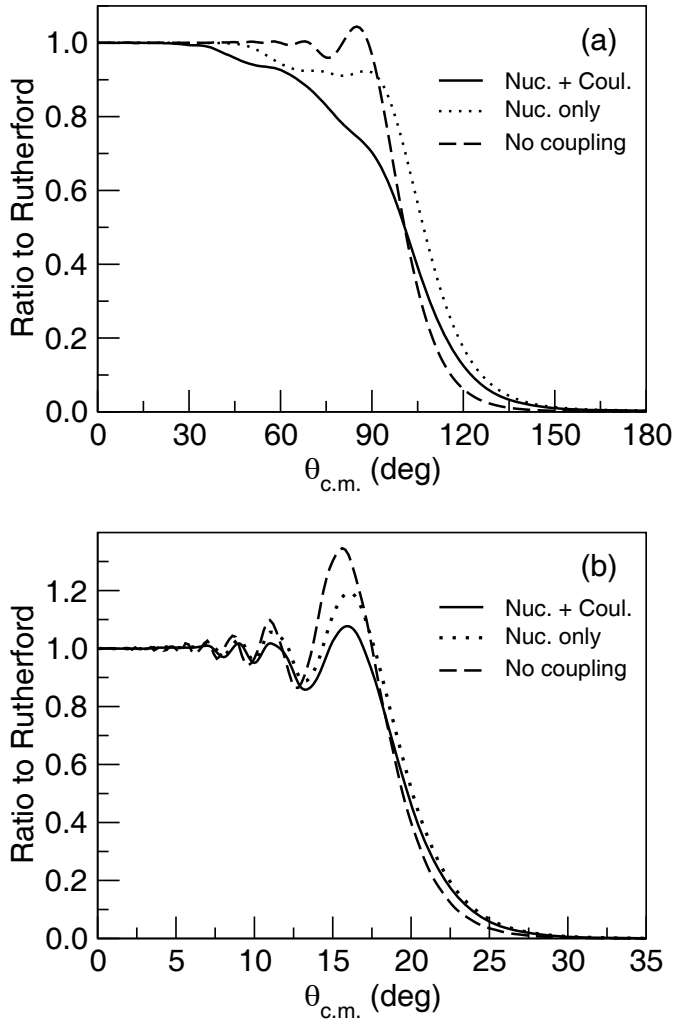

Fig. 22. (a) Coupled discretised continuum channels calculations for the $^{15}C + ^{208}Pb$ system at a bombarding energy of 65 MeV. The dashed curve denotes the no coupling optical model calculation while the solid curve denotes the coupled discretised continuum channels calculation including coupling to the $^{14}C + n$ continuum. The dotted curve denotes a coupled discretised continuum channels calculation with nuclear couplings only. (b) Similar calculations for an incident ^{15}C energy of 190 MeV, equivalent to approximately three times the nominal Coulomb barrier for the $^{15}C + ^{208}Pb$ system. Note the different angular ranges.

Figure 21 shows that the single neutron stripping alone would be expected to give the characteristic "strong coupling" shape to the elastic scattering angular distribution in this system. However, the weak binding of ^{15}C implies that breakup coupling to the continuum could produce a similar effect. In fig. 22(a) we present the result of a coupled discretised continuum channels calculation for $^{15}C + ^{208}Pb$ at an incident energy of 65 MeV. The calculations are based on the same Watanabe-type folding procedure as was used to calculate the entrance channel potential in the coupled reaction channels calculation. Couplings to the $L = 0$, 1, 2, 3 and 4 $^{14}C + n$ continuum as well as the 0.74 MeV $5/2^+$ bound first excited state of ^{15}C were included with couplings up to multipolarity $\lambda = 4$. The continuum was divided into bins in momentum (k) space of width $\Delta k = 0.1\,\mathrm{fm}^{-1}$ up to a maximum value $k_{\max} = 0.6\,\mathrm{fm}^{-1}$. The calculated angular distribution exhibits the strong coupling shape typical of other weakly bound radioactive beams scattered from heavy targets. Also plotted on fig. 22(a), as the dotted curve, is the result of a coupled discretised continuum channels calculation with nuclear coupling potentials only (diagonal Coulomb potentials were retained). It will be noted that the nuclear couplings are important for ^{15}C, suggesting that it is more similar to ^{11}Be than to ^{6}He or ^{11}Li where the Coulomb couplings are dominant. However, the trade off between nuclear and Coulomb couplings is to some extent energy dependent, and test calculations for $^{11}Li + ^{208}Pb$ for an incident energy of 40 MeV yield a relative importance for nuclear and Coulomb coupling similar to that for 65 MeV $^{15}C + ^{208}Pb$ shown in fig. 22(a), suggesting that ^{6}He may be more exceptional than at first thought in that Coulomb breakup couplings appear to be dominant over the whole range of near-barrier energies, see fig. 12 and fig. 1(c) of ref. [35], for example. More data (and more sophisticated calculations) are clearly desirable to investigate further this fascinating question.

The near barrier $^{15}C + ^{208}Pb$ elastic scattering is therefore expected to exhibit strong coupling effects both on account of couplings to the continuum and strong single neutron stripping couplings. In this respect it should be somewhat similar to the recent data for near-barrier $^{8}He + ^{208}Pb$ elastic scattering [31]. However, fig. 22(b) underlines the necessity of performing the measurements at energies close to the Coulomb barrier. Figure 22(b) presents the result of a similar coupled discretised continuum channels calculation to that shown in fig. 22(a) but for an incident ^{15}C energy of 190 MeV, approximately three times the nominal Coulomb barrier for this system. The continuum was extended up to a maximum value $k_{\max} = 1.2\,\mathrm{fm}^{-1}$, the bins for k values above $0.6\,\mathrm{fm}^{-1}$ being of width $\Delta k = 0.2\,\mathrm{fm}^{-1}$. The predicted elastic scattering angular distribution is now seen to be of an essentially standard Fresnel type pattern with a slight residual strong Coulomb coupling effect just before the main Coulomb-nuclear interference peak, similar to that of the 161.2 MeV $^{20}Ne + ^{208}Pb$ data of fig. 5(b).

5.4 Heavier radioactive beams on a heavy target

Many heavier not weakly bound radioactive nuclei are either known to be or are predicted to be more strongly deformed than the corresponding isotopes in the valley of stability. As such they should also be interesting candidates for strong coupling effects on their elastic scattering from heavy targets. As examples we take ^{30}Ne and ^{32}Mg, both with lower lying and more strongly coupled first excited states than their already strongly coupled stable counterparts ^{20}Ne and ^{24}Mg. In fig. 23 we present the result of a coupled channels calculation for the elastic scattering of ^{30}Ne from a ^{208}Pb target at an incident ^{30}Ne energy of 131 MeV. The optical model potential parameters

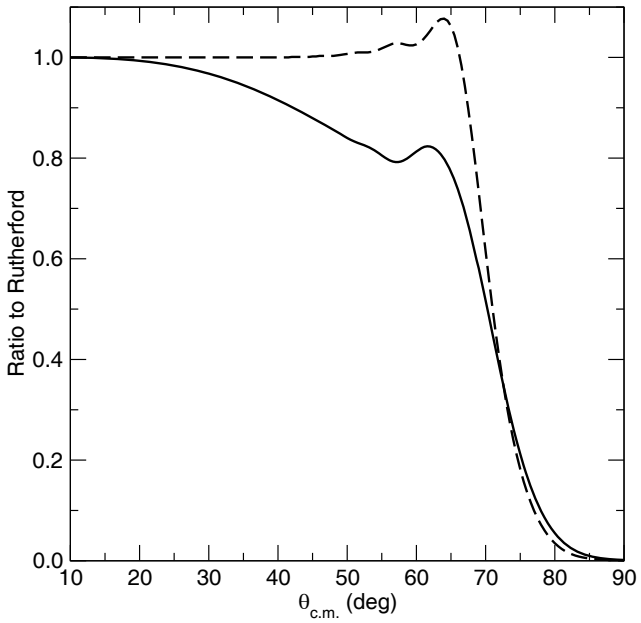

Fig. 23. Coupled channels calculation for the $^{30}\mathrm{Ne} + {}^{208}\mathrm{Pb}$ system at an incident ^{30}Ne energy of 131 MeV. The solid curve denotes the result of a coupled channels calculation including coupling to the 2_1^+ state of ^{30}Ne only while the dashed curve denotes a no coupling optical model calculation using the same optical potential as in the coupled channels calculation.

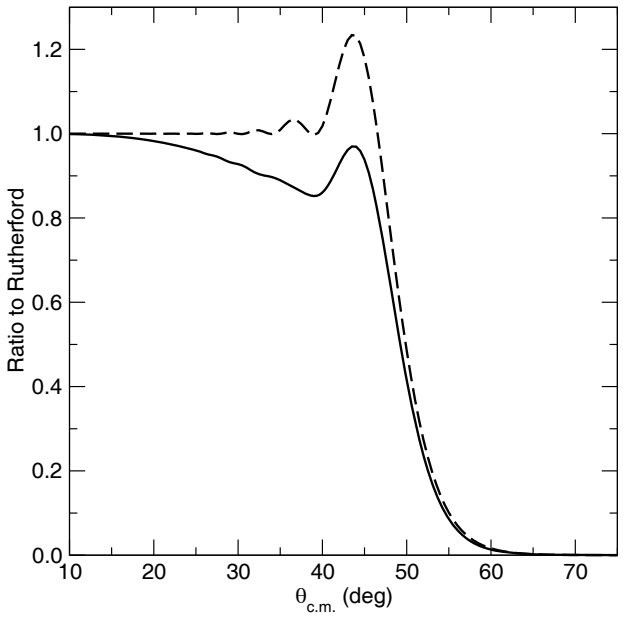

Fig. 24. Coupled channels calculation for the $^{32}\mathrm{Mg} + {}^{208}\mathrm{Pb}$ system at an incident ^{32}Mg energy of 200 MeV. The solid curve denotes the result of a coupled channels calculation including coupling to the 2_1^+ state of ^{32}Mg only while the dashed curve denotes a no coupling optical model calculation using the same optical potential as in the coupled channels calculation.

are the same as those used in the 131 MeV $^{20}\mathrm{Ne} + {}^{208}\mathrm{Pb}$ calculation shown in fig. 5 and the $B(E2)$ value was taken from ref. [62]. The nuclear deformation length was derived from the $B(E2)$ assuming the collective model expression and a charge radius of $1.2 \times A^{1/3}$ fm; this value was then multiplied by a factor of 0.75 before insertion in the coupled channels calculation since nuclear deformation lengths derived from fits to inelastic scattering data tend to be somewhat smaller than the values derived from the corresponding $B(E\lambda)$. As a comparison of figs. 5 and 23 will show, the coupling effect for ^{30}Ne is considerably larger than that for ^{20}Ne at the same energy. While fig. 23 should not be taken as a quantitatively reliable prediction —there may be additional effects due to strong transfer couplings and differences in the underlying optical potential parameters for ^{30}Ne compared to ^{20}Ne— it does demonstrate that ^{30}Ne would be an interesting candidate for study when beams becomes available.

In fig. 24 we present the results of a similar calculation for the $^{32}\mathrm{Mg} + {}^{208}\mathrm{Pb}$ system at an incident ^{32}Mg energy of 200 MeV. The optical model potential parameters were taken from a coupled channels fit to the 200 MeV $^{24}\mathrm{Mg} + {}^{208}\mathrm{Pb}$ elastic scattering data of ref. [11], which included coupling to the 2_1^+ state of ^{24}Mg only. The ^{32}Mg $B(E2)$ was again taken from ref. [62] and the nuclear deformation length derived in a similar way to the $^{30}\mathrm{Ne} + {}^{208}\mathrm{Pb}$ calculations. The coupling effect is considerably larger than for the $^{24}\mathrm{Mg} + {}^{208}\mathrm{Pb}$ system at the same energy although the same caveats apply to the quantitative reliability of the prediction as for the $^{30}\mathrm{Ne} + {}^{208}\mathrm{Pb}$ case.

6 Discussion

We have shown in this review that strong coupling effects on near-barrier heavy ion elastic scattering have a long history, going back nearly forty years. The important point to draw from the large body of work of this type conducted with stable beams is that the elastic scattering can, under the right conditions, be sensitive to the nuclear structure of the colliding nuclei, projectile or target or both. The advent of beams of weakly bound light radioactive nuclei at suitable energies (and of suitable quality) has led to a revival of interest in this topic, see for example ref. [66] for a recent article.

In addition to its intrinsic interest from the point of view of studies of the reaction mechanism, measurements of the elastic scattering for systems where the "strong coupling effect" is apparent may have other uses. The sensitivity of the elastic scattering angular distribution to the details of the nuclear structure may be exploited as a means of extracting nuclear structure information, in particular the $B(E\lambda)$ value for the strongly coupled state. This was already suggested in the context of the application of an analytical form of the long-ranged Coulomb DPP by Baltz *et al.*, [50]: "Indeed, in the situation where the long-range potential arises dominantly from a single state, sub-Coulomb elastic scattering analyzed in terms of our analytical expression might provide an alternative method of determining the experimental $B(E2)$ to that single state" [50].

While we would not advocate such measurements as a replacement for the traditional methods such as Coulomb

excitation, for suitable radioactive beams a measurement of the near-barrier elastic scattering from an appropriate target might provide a valuable adjunct. The method has much to recommend it, since in the case of the $^{18}O + ^{184}W$ system the coupling effect on the elastic scattering was almost exclusively due to the Coulomb coupling to the 2_1^+ state of ^{184}W and was thus sensitive to the $B(E2)$ value for excitation of this state; the other members of the rotational band seemed to have little or no influence. The same was found for the $^{20}Ne + ^{208}Pb$ elastic scattering where the ^{20}Ne 2_1^+ was the relevant state; coupling to the 4_1^+ state had little or no effect on the elastic scattering (unlike the inelastic scattering to the ^{20}Ne 2_1^+). However, practical considerations linked with the likely quality of medium to heavy mass radioactive beams will severely limit the utility of the method, since it is essential that pure elastic scattering is measured, thus requiring good detection energy resolution.

That the near-barrier elastic scattering angular distribution can, under the right circumstances, clearly show differences due to the details of the nuclear structure of the interacting nuclei is demonstrated by fig. 25. The main influence on the elastic scattering is due to coupling to the 2_1^+ state of the projectile. In ^{20}Ne the 2_1^+ state has an excitation energy of 1.63 MeV and the $B(E2; 0_1^+ \rightarrow 2_1^+) = 0.034\,e^2b^2$ [60], whereas in ^{22}Ne the 2_1^+ excitation energy is 1.27 MeV and the $B(E2; 0_1^+ \rightarrow 2_1^+) = 0.023\,e^2b^2$ [60]. This difference between the two isotopes translates to an effect of order 10% in the measured elastic scattering angular distributions in the region of the Coulomb-nuclear interference peak and as fig. 25 shows, the precision required clearly to demonstrate the effect is well within the capabilities of measurements with stable beams. However, effects of this order should also be visible in measurements with radioactive beams of the quality now becoming available and which will be available at the second generation radioactive beam facilities when these come on line (a precision of between 2–3% in measurements of elastic scattering angular distributions has already been achieved with some currently available radioactive beams, notably ^6He).

With the continuing development of existing radioactive ion beam facilities including advanced detector system updates, the future for these studies is bright. Further exploration of possible strong coupling effects due to transfer reactions should be particularly propitious. However, we emphasise that care is needed in the selection of beam and target combinations and the choice of incident energy; it is clear from the data and calculations presented in this review that a beam energy close to the nominal Coulomb barrier for the system under study is essential if strong coupling effects on the elastic scattering are to be observed unambiguously. The one exception to this rule seems to be ^{11}Li, where the coupling to the continuum is so strong that it should persist to energies well in excess of the Coulomb barrier, at least for heavy targets. On the other hand, in ^8B we have the intriguing case of a nucleus which ought to be exotic —it has the lowest known threshold against breakup and the predicted breakup cross sections are very large— and yet is not, at least not in the conventional sense, since coupling to the $^7Be + p$ continuum has an almost negligible effect in coupled discretised continuum channels calculations. Why this should be so remains "a riddle, wrapped in a mystery, inside an enigma" [68]. One might almost say that ^8B is exotic because it is *not* exotic... Nevertheless, it is clear that much work remains to be done in this fascinating field, proving that elastic scattering measurements are neither trivial nor uninteresting.

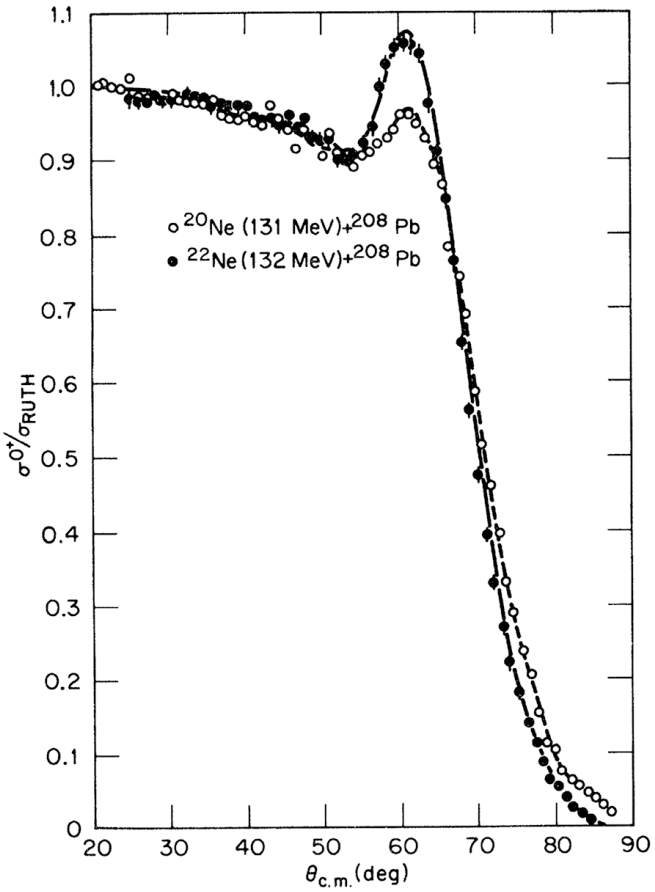

Fig. 25. Elastic scattering angular distributions for 131 MeV $^{20}Ne + ^{208}Pb$ and 132 MeV $^{22}Ne + ^{208}Pb$. The solid curves denote coupled channels fits including couplings to the 0_1^+, 2_1^+ and 4_1^+ states of ^{20}Ne and ^{22}Ne, see ref. [67] for details. Taken from ref. [67]. Reprinted fig. 1 with permission from [67]. © 1984, The American Physical Society.

The authors would like to thank Dr. D.D. Caussyn for help with scanning figures for this article. KWK acknowledges partial support from the Florida State University Robert O. Lawton Fund. Figures 8 and 10 are © 1984 and 1992, respectively, reprinted with permission from Elsevier.

References

1. V.P. Rudakov, K.P. Artemov, Yu.A. Glukhov, S.A. Goncharov, A.S. Demyanova, A.A. Ogloblin, V.V. Paramonov, M.V. Rozhkov, Bull. Rus. Acad. Sci. Phys. **65**, 57 (2001).
2. C.E. Thorn, M.J. LeVine, J.J. Kolata, C. Flaum, P.D. Bond, J.-C. Sens, Phys. Rev. Lett. **38**, 384 (1977).
3. E.E. Gross, T.P. Cleary, J.L.C. Ford, D.C. Hensley, K.S. Toth, Phys. Rev. C **17**, 1665 (1978).
4. G.R. Satchler, Phys. Lett. B **55**, 167 (1975).
5. J.B. Ball, C.B. Fulmer, E.E. Gross, M.L. Halbert, D.C. Hensley, C.A. Ludemann, M.J. Saltmarsh, G.R. Satchler, Nucl. Phys. A **252**, 208 (1975).
6. B.-T. Kim, Phys. Lett. B **80**, 353 (1979).
7. R.G. Stokstad, E.E. Gross, Phys. Rev. C **23**, 281 (1981).
8. P. Talon, N. Alamanos, M. Lamehi-Rachti, C. Levi, L. Papineau, Nucl. Phys. A **359**, 493 (1981).
9. D. Abriola, D. DiGregorio, J.E. Testoni, A. Etchegoyen, M.C. Etchegoyen, J.O. Fernández Niello, A.M.J. Ferrero, S. Gil, A.O. Macchiavelli, A.J. Pacheco, J. Kittl, Phys. Rev. C **39**, 546 (1989).
10. J.S. Eck, T.R. Ophel, P.D. Clark, D.C. Weisser, G.R. Satchler, Phys. Rev. C **23**, 228 (1981).
11. D.C. Hensley, E.E. Gross, M.L. Halbert, J.R. Beene, F.E. Bertrand, G. Vourvopoulos, D.L. Humphrey, T. Van Cleve, Phys. Rev. C **40**, 2065 (1989).
12. D.C. Hensley, E.E. Gross, M.L. Halbert, J.R. Beene, F.E. Bertrand, G. Vourvopoulos, D.L. Humphrey, Phys. Rev. C **43**, 2546 (1991).
13. R.J. Vojtech, J.J. Kolata, L.A. Lewandowski, K.E. Rehm, D.G. Kovar, G.S.F. Stephans, G. Rosner, H. Ikezoe, M.F. Vineyard, Phys. Rev. C **35**, 2139 (1987).
14. P.R. Christensen, S. Pontoppidan, F. Videbaek, J. Barrette, P.D. Bond, Ole Hansen, C.E. Thorn, Phys. Rev. C **29**, 455 (1984).
15. J.J. Kolata, K.E. Rehm, D.G. Kovar, G.S.F. Stephans, G. Rosner, H. Ikezoe, R. Vojtech, Phys. Rev. C **30**, 125 (1984).
16. C-L. Jiang, S. Kubono, N. Ikeda, M. Tanaka, H. Kawashima, Y. Fuchi, I. Katayama, T. Nomura, S.C. Pieper, Phys. Lett. B **259**, 427 (1991).
17. D. Fick, G. Grawert, I.M. Turkiewicz, Phys. Rep. **214**, 1 (1992).
18. H. Nishioka, J.A. Tostevin, R.C. Johnson, K.-I. Kubo, Nucl. Phys. A **415**, 230 (1984).
19. K. Rusek, Z. Moroz, R. Caplar, P. Egelhof, K.-H. Möbius, E. Steffens, I. Koenig, A. Weller, D. Fick, Nucl. Phys. A **407**, 208 (1983).
20. K. Rusek, N.M. Clarke, R.P. Ward, Phys. Rev. C **50**, 2010 (1994).
21. S.P. Van Verst, D.P. Sanderson, D.E. Trcka, K.W. Kemper, V. Hnizdo, B.G. Schmidt, K.R. Chapman, Phys. Rev. C **39**, 853 (1989).
22. J.A. Ruiz, J.L. Ferrero, B. Bilwes, R. Bilwes, Nucl. Phys. A **548**, 510 (1992).
23. U. Arlt, R. Bass, V. Hartmann, R. Renfordt, K. Sapotta, P. Fröbrich, W. Schäfer, Phys. Rev. C **22**, 1790(R) (1980).
24. M. Beckerman, R.L. Auble, F.E. Bertrand, J.L. Blankenship, B.L. Burks, M.A.G. Fernandes, C.W. Glover, E.E. Gross, D.J. Horen, R.O. Sayer, G.R. Satchler, D. Shapira, Y. Sugiyama, R.L. Varner, Phys. Rev. C **36**, 657 (1987).
25. S. Szilner, L. Corradi, F. Haas, G. Pollarolo, S. Beghini, B.R. Behera, E. Caurier, E. Fioretto, A. Gadea, A. Latina, G. Montagnoli, F. Nowacki, F. Scarlassara, A.M. Stefanini, M. Trotta, A.M. Vinodkumar, Y.W. Wu, Eur. Phys. J. A **21**, 87 (2004).
26. N. Keeley, N. Alamanos, K.W. Kemper, K. Rusek, Prog. Part. Nucl. Phys. **63**, 396 (2009).
27. O.R. Kakuee, J. Rahighi, A.M. Sánchez-Benítez, M.V. Andrés, S. Cherubini, T. Davinson, W. Galster, J. Gómez-Camacho, A.M. Laird, M. Lamehi-Rachti, I. Martel, A.C. Shotter, W.B. Smith, J. Vervier, P.J. Woods, Nucl. Phys. A **728**, 339 (2003).
28. A. Di Pietro, P. Figuera, F. Amorini, C. Angulo, G. Cardella, S. Cherubini, T. Davinson, D. Leanza, J. Lu, H. Mahmud, M. Milin, A. Musumarra, A. Ninane, M. Papa, M.G. Pellegriti, R. Raabe, F. Rizzo, C. Ruiz, A.C. Shotter, N. Soic, S. Tudisco, Europhys. Lett. **64**, 309 (2003).
29. A. Di Pietro, P. Figuera, F. Amorini, C. Angulo, G. Cardella, S. Cherubini, T. Davinson, D. Leanza, J. Lu, H. Mahmud, M. Milin, A. Musumarra, A. Ninane, M. Papa, M.G. Pellegriti, R. Raabe, F. Rizzo, C. Ruiz, A.C. Shotter, N. Soic, S. Tudisco, L. Weissman, Phys. Rev. C **69**, 044613 (2004).
30. Y. Kucuk, I. Boztosun, N. Keeley, Phys. Rev. C **79**, 067601 (2009).
31. G. Marquínez-Durán, A.M. Sánchez-Benítez, I. Martel, L. Acosta, K. Rusek, M.A.G. Álvarez, R. Berjillos, M.J.G. Borge, A. Chbihi, C. Cruz, M. Cubero, J.A. Dueñas, J.P. Fernández-García, B. Fernández-Martínez, J.L. Flores, J. Gómez-Camacho, N. Keeley, J.A. Labrador, M. Marqués, A.M. Moro, M. Mazzocco, A. Pakou, V.V. Parkar, N. Patronis, V. Pesudo, D. Pierroutsakou, R. Raabe, R. Silvestri, N. Soic, Ł. Standylo, I. Strojek, O. Tengblad, R. Wolski, A.H. Ziad, Acta Phys. Pol. B **44**, 467 (2013).
32. L. Acosta, A.M. Sánchez-Benítez, M.E. Gómez, I. Martel, F. Pérez-Bernal, F. Pizarro, J. Rodríguez-Quintero, K. Rusek, M.A.G. Alvarez, M.V. Andrés, J.M. Espino, J.P. Fernández-García, J. Gómez-Camacho, A.M. Moro, C. Angulo, J. Cabrera, E. Casarejos, P. Demaret, M.J.G. Borge, D. Escrig, O. Tengblad, S. Cherubini, P. Figuera, M. Gulino, M. Freer, C. Metelko, V. Ziman, R. Raabe, I. Mukha, D. Smirnov, O.R. Kakuee, J. Rahighi, Phys. Rev. C **84**, 044604 (2011).
33. N. Keeley, N. Alamanos, Phys. Rev. C **77**, 054602 (2008).
34. M. Cubero, J.P. Fernández-García, M. Rodríguez-Gallardo, L. Acosta, M. Alcorta, M.A.G. Alvarez, M.J.G. Borge, L. Buchmann, C.A. Diget, H. Al Falou, B.R. Fulton, H.O.U. Fynbo, D. Galaviz, J. Gómez-Camacho, R. Kanungo, J.A. Lay, M. Madurga, I. Martel, A.M. Moro, I. Mukha, T. Nilsson, A.M. Sánchez-Benítez, A. Shotter, O. Tengblad, P. Walden, Phys. Rev. Lett. **109**, 262701 (2012).
35. N. Keeley, K.W. Kemper, K. Rusek, Phys. Rev. C **88**, 017602 (2013).
36. A. Di Pietro, G. Randisi, V. Scuderi, L. Acosta, F. Amorini, M.J.G. Borge, P. Figuera, M. Fisichella, L.M. Fraile, J. Gomez-Camacho, H. Jeppesen, M. Lattuada, I. Martel, M. Milin, A. Musumarra, M. Papa, M.G. Pellegriti, F. Perez-Bernal, R. Raabe, F. Rizzo, D. Santonocito, G. Scalia, O. Tengblad, D. Torresi, A.M. Vidal, D. Voulot, F. Wenander, M. Zadro, Phys. Rev. Lett. **105**, 022701 (2010).
37. N. Keeley, N. Alamanos, K.W. Kemper, K. Rusek, Phys. Rev. C **82**, 034606 (2010).

38. A. Di Pietro, V. Scuderi, A.M. Moro, L. Acosta, F. Amorini, M.J.G. Borge, P. Figuera, M. Fisichella, L.M. Fraile, J. Gomez-Camacho, H. Jeppesen, M. Lattuada, I. Martel, M. Milin, A. Musumarra, M. Papa, M.G. Pellegriti, F. Perez-Bernal, R. Raabe, G. Randisi, F. Rizzo, G. Scalia, O. Tengblad, D. Torresi, A.M. Vidal, D. Voulot, F. Wenander, M. Zadro, Phys. Rev. C **85**, 054607 (2012).
39. N.C. Summers, F.M. Nunes, I.J. Thompson, Phys. Rev. C **74**, 014606 (2006).
40. N.C. Summers, F.M. Nunes, I.J. Thompson, Phys. Rev. C **89**, 069901(E) (2014).
41. R. de Diego, J.M. Arias, J.A. Lay, A.M. Moro, Phys. Rev. C **89**, 064609 (2014).
42. Y.Y. Yang, J.S. Wang, Q. Wang, D.Y. Pang, J.B. Ma, M.R. Huang, J.L. Han, P. Ma, S.L. Jin, Z. Bai, Q. Hu, L. Jin, J.B. Chen, N. Keeley, K. Rusek, R. Wada, S. Mukherjee, Z.Y. Sun, R.F. Chen, X.Y. Zhang, Z.G. Hu, X.H. Yuan, X.G. Cao, Z.G. Xu, S.W. Xu, C. Zhen, Z.Q. Chen, Z. Chen, S.Z. Chen, C.M. Du, L.M. Duan, F. Fu, B.X. Gou, J. Hu, J.J. He, X.G. Lei, S.L. Li, Y. Li, Q.Y. Lin, L.X. Liu, F.D. Shi, S.W. Tang, G. Xu, X. Xu, L.Y. Zhang, X.H. Zhang, W. Zhang, M.H. Zhao, Z.Y. Guo, Y.H. Zhang, H.S. Xu, G.Q. Xiao, Phys. Rev. C **87**, 044613 (2013).
43. J. Lubian, T. Correa, E.F. Aguilera, L.F. Canto, A. Gomez-Camacho, E.M. Quiroz, P.R.S. Gomes, Phys. Rev. C **79**, 064605 (2009).
44. E.F. Aguilera, E. Martinez-Quiroz, D. Lizcano, A. Gómez-Camacho, J.J. Kolata, L.O. Lamm, V. Guimarães, R. Lichtenthäler, O. Camargo, F.D. Becchetti, H. Jiang, P.A. DeYoung, P.J. Mears, T.L. Belyaeva, Phys. Rev. C **79**, 021601 (2009).
45. R. Kumar, A. Bonaccorso, Phys. Rev. C **84**, 014613 (2011).
46. R. Kumar, A. Bonaccorso, Phys. Rev. C **86**, 061601(R) (2012).
47. N. Keeley, R.S. Mackintosh, C. Beck, Nucl. Phys. A **834**, 792c (2010).
48. W.G. Love, T. Terasawa, G.R. Satchler, Phys. Rev. Lett. **39**, 6 (1977).
49. W.G. Love, T. Terasawa, G.R. Satchler, Nucl. Phys. A **291**, 183 (1977).
50. A.J. Baltz, S.K. Kauffmann, N.K. Glendenning, K. Pruess, Phys. Rev. Lett. **40**, 20 (1978).
51. A.J. Baltz, N.K. Glendenning, S.K. Kauffmann, K. Pruess, Nucl. Phys. A **327**, 221 (1979).
52. G.R. Satchler, *Direct Nuclear Reactions* (Clarendon Press, Oxford, 1987).
53. R.S. Mackintosh, N. Keeley, Phys. Rev. C **79**, 014611 (2009).
54. V.V. Parkar, I. Martel, A.M. Sánchez-Benítez, L. Acosta, K. Rusek, Ł. Standylo, N. Keeley, Acta Phys. Pol. B **42**, 761 (2011).
55. M.V. Andrés, J. Gómez-Camacho, M.A. Nagarajan, Nucl. Phys. A **579**, 273 (1994).
56. W.E. Frahn, T.F. Hill, Z. Phys. A **285**, 315 (1978).
57. K. Rusek, Eur. Phys. J. A **41**, 399 (2009).
58. I.J. Thompson, Comput. Phys. Rep. **7**, 167 (1988).
59. R.A. Broglia, A. Winther, *Heavy Ion Reaction Lecture Notes*, Vol. **1**: *Elastic and Inelastic Reactions* (Benjamin/Cummings, Reading, 1981).
60. S. Raman, C.W. Nestor, Jr., P. Tikkanen, At. Data Nucl. Data Tables **78**, 1 (2001).
61. T. Kibédi, R.H. Spear, At. Data Nucl. Data Tables **80**, 35 (2002).
62. B. Pritychenko, M. Birch, B. Singh, M. Horoi, Nucl. Data Sheets **120**, 111 (2014) arXiv:1312.5975 [nucl-th].
63. N. Keeley, N. Alamanos, Phys. Rev. C **75**, 054610 (2007).
64. S. Santra, P. Singh, S. Kailas, A. Chatterjee, A. Shrivastava, K. Mahata, Phys. Rev. C **64**, 024602 (2001).
65. J.R.M. Annand, R.W. Finlay, F.S. Dietrich, Nucl. Phys. A **443**, 249 (1985).
66. A. Diaz-Torres, A.M. Moro, Phys. Lett. B **733**, 89 (2014).
67. E.E. Gross, T.P. Cleary, J.L.C. Ford, Jr., D.C. Hensley, K.S. Toth, F.T. Baker, A. Scott, C.R. Bingham, J.A. Vrba, Phys. Rev. C **29**, 459 (1984).
68. W.S. Churchill, speech broadcast on 1st October 1939.

Nicholas Keeley obtained his PhD in experimental nuclear physics from the University of Birmingham in 1993 and habilitation from the Andrzej Sołtan Institute for Nuclear Studies in 2011. He is currently an Associate Professor in the Nuclear Physics Division of the National Centre for Nuclear Research in Warsaw.

Kirby W. Kemper is a Robert O. Lawton Professor of Physics (Emeritus) at Florida State University. He has participated in nuclear physics experiments at various laboratories around the world including those at the Florida State University John D. Fox Accelerator Laboratory. His current interest is in understanding the structure of very neutron-rich nuclei.

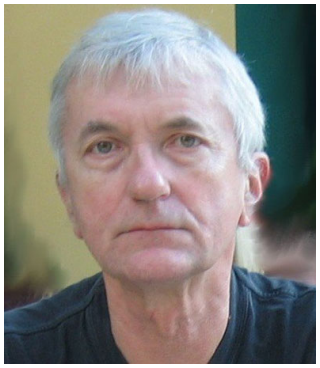

Krzysztof Rusek received his Habilitation in 1998 from the Andrzej Sołtan Institute for Nuclear Studies where he worked for many years. He was a post-doc at the Max Planck Institute of Nuclear Physics in Heidelberg and at the University of Birmingham. For the past few years he has served as director of the Heavy Ion Laboratory of the University of Warsaw. He is a nuclear physicist specialising in nuclear reactions with light, weakly bound nuclei.